AFAL-TR-88-072

AD:

(4)

Final Report
for the period
October 1986 to
July 1988

Kinetic Deuterium Isotope Effects in the Combustion of Nitramine Propellants

AD-A199 760

July 1988

Author:
Paul C. Trulove

Approved for Public Release

**Air Force
Astronautics
Laboratory**

Air Force Space Technology Center
Space Division, Air Force Systems Command
Edwards Air Force Base,
California 93523-5000

NOTICE

When U.S. Government drawings, specifications, or other data are used for any purpose other than a definitely related Government procurement operation, the fact that the Government may have formulated, furnished, or in any way supplied the said drawings, specifications, or other data, is not to be regarded by implication or otherwise, or in any way licensing the holder or any other person or corporation, or conveying any rights or permission to manufacture, use, or sell any patented invention that may be related thereto.

FOREWORD

This final report documents a study on the Kinetic Deuterium Isotype Effects in the Combustion of Nitramine Propellants at the Air Force Astronautics Laboratory (AFAL), Edwards Air Force Base, CA. AFAL Project Manager was Paul Trulove.

This report has been reviewed and is approved for release and distribution in accordance with the distribution statement on the cover and on the DD Form 1473.

PAUL C. TRULOVE, CAPT, USAF
Project Manager

WILLIAM C. RURLEY, MAJOR, USAF
Chief, Chemistry and Material Branch

FOR THE COMMANDER

ROBERT C. CORLEY
Deputy Chief, Astronautical Sciences Division

SECURITY CLASSIFICATION OF THIS PAGE

REPORT DOCUMENTATION PAGE

Form Approved OMB No. 0704-0188

1a. REPORT SECURITY CLASSIFICATION: UNCLASSIFIED	1b. RESTRICTIVE MARKINGS
2a. SECURITY CLASSIFICATION AUTHORITY	3. DISTRIBUTION/AVAILABILITY OF REPORT: Approved for public release, distribution is unlimited.
2b. DECLASSIFICATION/DOWNGRADING SCHEDULE	
4. PERFORMING ORGANIZATION REPORT NUMBER(S): AFAL-TR-88-072	5. MONITORING ORGANIZATION REPORT NUMBER(S)
6a. NAME OF PERFORMING ORGANIZATION: Air Force Astronautics Laboratory; 6b. OFFICE SYMBOL (If applicable): LSSP	7a. NAME OF MONITORING ORGANIZATION
6c. ADDRESS (City, State, and ZIP Code): Edwards AFB CA 93523-5000	7b. ADDRESS (City, State, and ZIP Code)
8a. NAME OF FUNDING/SPONSORING ORGANIZATION; 8b. OFFICE SYMBOL (If applicable)	9. PROCUREMENT INSTRUMENT IDENTIFICATION NUMBER
8c. ADDRESS (City, State, and ZIP Code)	10. SOURCE OF FUNDING NUMBERS

PROGRAM ELEMENT NO.	PROJECT NO.	TASK NO	WORK UNIT ACCESSION NO.
61102F	2303	M1	ST

11. TITLE (Include Security Classification): Kinetic Deuterium Isotope Effects in the Combustion of Nitramine Propellants (U)

12. PERSONAL AUTHOR(S): Trulove, Paul C.

13a. TYPE OF REPORT	13b. TIME COVERED	14. DATE OF REPORT (Year, Month, Day)	15. PAGE COUNT
Final	FROM 86/10 TO 88/7	88/7	117

16. SUPPLEMENTARY NOTATION

17. COSATI CODES		
FIELD	GROUP	SUB-GROUP
21	09	2
21	02	

18. SUBJECT TERMS (Continue on reverse if necessary and identify by block number): HMX, RDX, Combustion, Isotope Effects, Mechanism, Rate-Limiting Reactions, Propellants, Nitramines.

19. ABSTRACT (Continue on reverse if necessary and identify by block number)

The deuterium isotope effect was used to investigate the rate limiting process in the combustion of nitramine propellants. Model propellant formulations containing either octahydro-1,3,5,7-tetranitro-1,3,5,7-tetrazocine (HMX), hexahydro-1,3,5-trinitro-1,3,5-triazine (RDX), or their deuteriated analogues were pressed into pellets and burned under nitrogen pressure in a window bomb. The magnitudes of the observed deuterium isotope effects indicate that the HMX and RDX exert significant control over the burning process of the studied propellants. Furthermore, assuming a consistent mechanism between decomposition and combustion, the observed isotope effects suggest that a carbon-hydrogen bond rupture in HMX and RDX is the rate controlling process in the combustion of the model nitramine propellants.

20. DISTRIBUTION/AVAILABILITY OF ABSTRACT: ☒ UNCLASSIFIED/UNLIMITED ☐ SAME AS RPT. ☐ DTIC USERS	21. ABSTRACT SECURITY CLASSIFICATION: UNCLASSIFIED
22a. NAME OF RESPONSIBLE INDIVIDUAL: Paul C. Trulove, Capt, USAF	22b. TELEPHONE (Include Area Code): (805) 275-5410; 22c. OFFICE SYMBOL: LSSP

DD Form 1473, JUN 86 — Previous editions are obsolete. — SECURITY CLASSIFICATION OF THIS PAGE

TABLE OF CONTENTS

LIST OF TABLES

LIST OF FIGURES

INTRODUCTION

Octahydro-1,3,5,7-tetranitro-1,3,5,7-tetrazocine (HMX) and hexahydro-1,3,5-trinitro-1,3,5-s-triazine (RDX) (Fig. 1) have been the focus of a great deal of research since their discovery around the turn of the century.[1,2] The acronym HMX, coined by researchers in Great Britain,[1] derives from the phrase "High Melting Explosive of His Majesty's Explosive." This code name was based on the fact that in the early syntheses of HMX, RDX was present as a major contaminant.[2] HMX was simply the higher melting of the two explosives. The acronym RDX, also a code name given by the British researchers, stands for "Research Department Explosive" or "Royal Demolition Explosive."

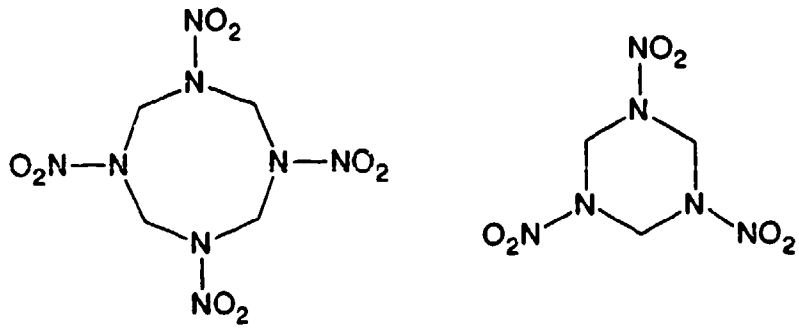

FIGURE 1. Structures of HMX and RDX

HMX and RDX are cyclic nitramines which are both high explosives. They posses an explosive force approximately one and a half times greater than TNT.[1,2] Both HMX and RDX have been used in munitions since before World War II, but it has been only in the past two decades that they have been employed in rocket propellants.

SOLID ROCKET PROPELLANTS

Solid rocket propellants consist primarily of three components: the fuel, the oxidizer, and the rubbery binder.[3] A typical solid rocket propellant is composed principally of powdered aluminum (Al) fuel, ammonium perchlorate (AP) oxidizer, and a crosslinked polybutadiene binder.

Solid propellant performance is normally quoted in terms of specific impulse (I_{sp}). The propellant thrust (F) and the mass flow rate of exhaust products (w) are related to I_{sp} by equation 1.[4]

$$I_{sp} = \frac{F}{w} \tag{1}$$

The unit of F is pounds (force), and the units of w are pounds (mass) per second. The unit of I_{sp} is normally given as seconds. However, the actual unit is feet per second. The I_{sp} of a typical Al/AP propellant ranges from 260 to 265 seconds.

The effect of pressure on the burn rate (r) of a propellant is given by

$$r = a(p_c)^n \tag{2}$$

where p_c is the pressure inside the combustion chamber, a is an empirical constant, and n is the burning rate pressure exponent.[3] The larger the pressure exponent the greater the change in propellant burn rate with increasing

pressure. An acceptable value for the pressure exponent falls between 0.2 and 0.8. In developing a propellant formulation one attempts to maximize the performance (i.e. the I_{sp}) while maintaining a reasonable pressure exponent.

Aluminum/ammonium perchlorate-based propellants produce copious amounts of smoke during combustion due to the presence of Al_2O_3 and HCl as combustion products. This type of highly visible exhaust plume can be a great disadvantage during a combat situation. Therefore, in recent years there has been a move toward low signature or minimum smoke propellants. Most of these propellants incorporate the nitramines, HMX or RDX, as replacements for both the fuel (Al) and the oxidizer (AP). Nitramine-based propellants give performance comparable to conventional Al/AP propellants, and their combustion produces only gaseous products giving them almost invisible exhaust plumes.

Unfortunately, nitramine based propellants possess certain problems which have thus far limited their application. To begin with, nitramine propellants tend to have large pressure exponents, often greater than 0.8. As a consequence the propellant burn rate and the combustion pressure are very sensitive to each other such that catastrophic pressure increases can occur in a few milliseconds.[3]

It is difficult to vary the burn rate of nitramine propellants through modification of the propellant formulation. Techniques developed to modify the burn rate of Al/AP propellants such as changing ingredient particle size, adding catalysts, varying the amounts of ingredients, etc., have little effect on the burn rate of nitramine propellants. In essence nitramine propellants tend to burn over a very narrow range often referred to as the "burn rate box". To make matters worse, the burn rates of nitramine propellants are normally too slow for most applications.

Al/AP-based propellants are normally in the 1.3 hazard classification range. However, because HMX and RDX are high explosives, propellants made from these nitramines tend to be relatively sensitive, and are normally in the 1.1 hazard classification (the classification 1.1 is for compounds that detonate whereas the classification 1.3 is for compounds that burn rapidly or deflagrate). The increased hazard of nitramine propellants presents significant handling problems and in general limits their application to land based systems.

If HMX and RDX based propellants are to be used on a broad scale significant improvements in the pressure exponent, burn rate range, and propellant hazard must be made. This, in turn, necessitates a fundamental understanding of the processes governing the energy release in the combustion of HMX and RDX.

HMX AND RDX RESEARCH

The initial work on HMX and RDX decomposition was published by Robertson[5] in 1949. Since that time a large body of work, some of which is summarized in the reviews,[6-15] has been devoted to studying all aspects of the thermal processes (decomposition, pyrolysis, deflagration, combustion, and detonation) of HMX and RDX. To a large extent these studies have simply generated a myriad of proposed mechanisms, attesting to the complex nature of these thermal reactions. Recently, researchers have focused their attentions on determining the rate limiting reactions in the thermal decomposition and high pressure combustion of HMX and RDX because it is the rate of the slowest reaction which to a large extent controls the global energy release process.

Kinetic isotope effects provide a powerful technique for the investigation of the rate controlling reactions of the thermal process of energetic materials. Recently, isotope effects have been used to study the thermal decomposition

and combustion of HMX and RDX.[16-20] The results of these experiments implicate a C-H bond rupture as the global rate controlling phenomena in these thermochemical reactions.

The isotope effects studies have important implications in the improvement of nitramine-based propellants. However, the relevance of results for pure HMX and RDX is limited because of the possibly significant influence that energetic propellant ingredients may exert on the mechanism of nitramine propellant combustion.

In a continuation of previous combustion work on HMX[16] and RDX[17], I will report isotope effects in the combustion of model nitramine propellants. These results will be compared to the results for the combustion of the pure nitramines in a effort to draw some conclusions about the effect of propellant ingredients on the nitramine combustion mechanism. Finally, possible explanations will be offered for the observed isotope effects and their kinetic implications.

KINETIC DEUTERIUM ISOTOPE EFFECT THEORY

Kinetic isotope effects are the primary tool used in this research to study the combustion kinetics of nitramines and nitramine based propellants. Thus, it is important to establish a clear theoretical understanding of kinetic isotope effects before conclusions can be made from our data. Furthermore, a theoretical foundation is needed such that a critical evaluation of previous isotope effect studies concerning the decomposition and combustion kinetics of energetic materials can be made.

A kinetic isotope effect refers to the change in the rate at which a molecule undergoes a specific reaction when an atom (or atoms) in the molecule is (are) replaced with a different isotope. Isotope effects are normally expressed as a ratio of rate constants. In the case of the substitution of deuterium for protium, the isotope effect is most often represented as k_H/k_D, where k_H is the rate constant for the molecule containing protium and k_D is the rate constant for the molecule containing deuterium.

According to the Born-Oppenheimer approximation, the potential energy surface of a molecule depends only on the attractions and repulsions of electronic and nuclear charges, not on nuclear mass.[21,22] Nuclear motion, on the other hand, does depend on the mass of the nucleus, and in turn the relative nuclear motion determines the vibrational energy content of the molecule.[23] Consequently, molecules differing only by isotopic substitution move on the same potential energy surface but differ in vibrational energy content. To a

large extent, it is this vibrational energy difference which gives rise to kinetic isotope effects.

Kinetic isotope effects have long been recognized for their potential in the study of reaction rates and mechanisms. Normal substituent effects do not always give a clear understanding of a system due to changes in the potential energy surface and possible mechanistic changes which occur when going from one substituent to another. The potential energy surface and the reaction mechanisms of molecules differing only by isotopic substitution are essentially the same. This allows kinetic isotope effects to be used to investigate the nature of a single potential energy surface and thus a single transition state.[23]

Isotope effects are categorized as being either primary or secondary. A primary (1°) isotope effect occurs when a bond to the isotopic atom is broken during the rate limiting step. Secondary (2°) isotope effects are those effects which do not involve the rupture of a bond to the isotopic atom. Primary isotope effects are generally larger than secondary effects. However, as we shall see, determining whether an observed isotope effect is primary or secondary is far from trivial.

For single step reactions, kinetic isotope effects are observed when bonds to an isotopic atom undergo changes when going to the activated complex. In the case of multi-step reactions, isotope effects will be seen if bonds to an isotopic atom undergo changes in a slow step of the reaction mechanism.

ORIGINS OF KINETIC ISOTOPE EFFECTS

The theoretical foundation for the treatment of kinetic isotope effects was first advanced by Bigeleisen and Mayer in 1947.[24] Kinetic isotope effect theory is based on the "transition state theory" of Eyring[25] which assumes that

reactants are in thermal equilibrium with an "activated complex" or "transition state." Furthermore, it is this activated complex which decomposes in the rate limiting step of the overall process into products.[26] Bigeleisen and Mayer employed the tenets of transition state theory coupled with statistical mechanics to derive relationships which provide a reasonable explanation for observed kinetic isotope effects

The following discussion focuses on the isotope effects arising when deuterium is substituted for protium, hereafter referred to as Kinetic Deuterium Isotope Effects (KDIE). For more detailed information the reader is directed to the reviews[23,26-32] listed in the reference section of this thesis.

Zero Point Energy

A great majority of kinetic isotope effects result from differences in zero point energy between normal and isotopically labeled molecules. Consequently, a brief explanation of the origin of zero point energy differences is necessary for a complete understanding of kinetic isotope effects.

For a molecule **A-H** where **H** is hydrogen and **A** is the remainder of the molecule, the energy levels for the vibrations of **A-H** will be given by

$$E = \left[n + \frac{1}{2}\right]h\nu \qquad (3)$$

where h is Planck's constant, n is the vibrational quantum, and ν is the A-H vibrational frequency. This of course assumes that the **A-H** stretch is an isolated vibration and not part of a normal mode. The lowest energy level ($n = 0$) is the zero point energy (E_0);[33,34] it is given by

$$E_0 = \frac{1}{2}h\nu \qquad (4)$$

At normal temperatures almost all molecules occupy the n = 0 vibrational energy level.[33,35]

Assuming **A-H** behaves like a harmonic oscillator, the vibrational frequency will be given by

$$\nu = \frac{1}{2\pi}\sqrt{\frac{k}{\mu}} \tag{5}$$

where **k** is the force constant for the particular vibrational motion, and μ is the reduced mass of **A-H**. If **A** is significantly larger than **H**, the infinite mass approximation[22] can be used to obtain

$$\nu = \frac{1}{2\pi}\sqrt{\frac{k}{m_H}} \tag{6}$$

where m_H is the mass of the hydrogen atom.

Combining equations 4 and 6 we obtain the following expression for the zero point energy of a vibration.

$$E_0 = \frac{h}{4\pi}\sqrt{\frac{k}{m_H}} \tag{7}$$

Molecules differing only in isotopic mass, such as **A-H** versus **A-D** where **D** is deuterium, move along the same potential energy surface. Since the vibrational force constants depend solely on this potential energy surface, they are the same for both **A-H** and **A-D**. Thus, with this in mind equation 7 can be reduced to

$$E_0 \propto \frac{1}{\sqrt{m}} \tag{8}$$

where m is the mass of the light atom (i.e., **H** or **D**). Consequently, the vibrations of **A-D** will have lower zero point energies than the vibrations of **A-H**.

KDIE in a Hydrogen Atom Transfer

In an effort to make a complex subject more understandable, further discussions of kinetic isotope theory will center on the isotope effects arising in

a simple hydrogen transfer reaction. The logic used in the followir.g discussion will be generally applicable to most primary and secondary KDIEs.

Consider the following reaction involving the transfer of a protium atom (H), or a deuterium atom (D) from molecule A to molecule B.[26]

$$AH(D) + B \rightleftharpoons A\cdots H(D)\cdots B \longrightarrow A + BH(D) \qquad (9)$$

(The discussion below will focus primarily on the reaction involving protium with the understanding that what is said is also true for deuterium.) Following transition state theory, AH and B are in thermal equilibrium with the activated complex A····H····B which subsequently decomposes into the products A and BH. Figure 2a[26,31,32] shows a representation of a potential energy surface for this reaction. The BH bond length is plotted versus the AH bond length. Energy is plotted perpendicular to the plane of the paper with the contours connecting points of equal energy. The outermost contours are the highest in energy with the energy of the contours decreasing towards the center. The line of minimum energy along which the transition state lies is represented by a dashed line and is the reaction path.

Figure 2b[31,32] represents the reaction path from Figure 2a with cross sections of the potential energy surface corresponding to the reactants, activated complex, and products. All three potential wells show positive curvature and thus positive force constants perpendicular to the reaction path. In the case of the activated complex, the potential well corresponds to a symmetric stretch (i.e., ←A····H····B→).

The potential energy surface (Fig. 2b) shows a neutral curvature in the direction of the reaction path for both the reactants and products, indicating a zero force constant for motion in that direction. Thus, there is no resistance to the extension of the AH–B distance for the reactants and the A–HB distance

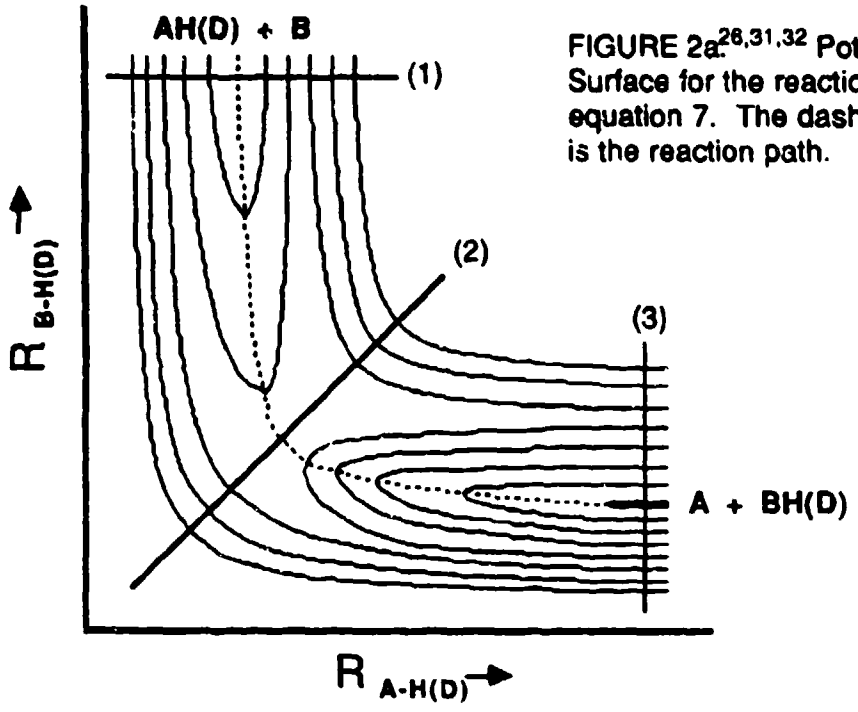

FIGURE 2a.[26,31,32] Potential Energy Surface for the reaction in equation 7. The dashed line is the reaction path.

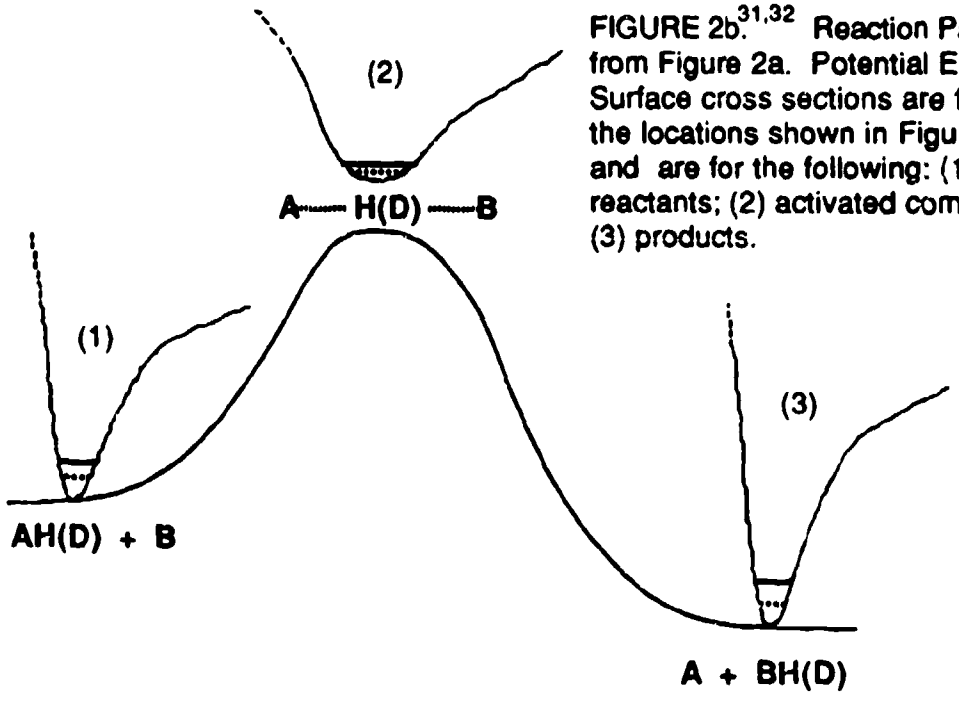

FIGURE 2b.[31,32] Reaction Path from Figure 2a. Potential Energy Surface cross sections are from the locations shown in Figure 1a and are for the following: (1) reactants; (2) activated complex; (3) products.

for the products. At the activated complex the potential energy surface shows a negative curvature along the reaction path. Consequently, motion of the activated complex along the reaction path, which corresponds to an asymmetric stretch (i.e., ←A····H→←B and A→←H····B→), is unstable. This follows directly from transition state theory, which requires that vibrational mode to become translation along the reaction path.[26,36]

The total zero point energy of a molecule is the sum of the zero point energies ($\frac{1}{2}h\nu$) of all the vibrational modes of the molecule. In the case of the product (A and BH) and the reactant (AH and B) molecules, the total zero point energies are the result of the contributions of the 3N-6 vibrational modes of these molecules, where N is the number of atoms in the molecule. The total zero point energy of the activated complex (A····H····B) is made up of the contributions of 3N-7 vibrational modes (one mode is lost to decomposition along the reaction path).[21,29] The solid line across the bottom portions of the three potential wells in Figure 1b represents the zero point energy level for the protiated molecules, and the dashed line represents the zero point energy level for the deuteriated molecules.

According to transition state theory, the rate constant k for a reaction is given by

$$k = \frac{k_B T}{h} \kappa \bar{K} \qquad (10)$$

where k_B is the Boltzmann constant, T is temperature, and h is Planck's constant. The transmission coefficient (κ) represents the probability that a given system moving in the direction of the reaction path will in fact pass over the potential energy barrier to the products side.[23] The quantity $\bar{K}$ is the equilibrium constant between the reactants and activated complex. For the hydrogen transfer reaction it takes the form of

$$\bar{K} = \frac{Q^{\ddagger}_{AHB}}{Q_{AH}Q_B} \exp\left[-\frac{E_a}{RT}\right] \tag{11}$$

where $Q^{\ddagger}_{AHB}$ is the partition function for the activated complex, Q_{AH} and Q_B are the molecular partition functions for the reactants, and R is the universal gas constant (the Cross of Lorraine (‡) is used to identify quantities associated with the activated complex/transition state). The activation energy for the reaction (E_a) is simply the difference between the zero point energy of the reactants (E_0) and the zero point energy of the activated complex ($E^{\ddagger}_0$).

Combining equations 10 and 11, the following expression for the rate constant of the hydrogen transfer reaction is obtained.

$$k = \frac{k_B T}{h} \kappa \frac{Q^{\ddagger}_{AHB}}{Q_{AH}Q_B} \exp\left[-\frac{E_a}{RT}\right] \tag{12}$$

As was pointed out earlier, KDIEs are represented as ratios of rate constants (i.e., k_H/k_D). Thus, if we take the ratio of the rate constant expressions for the protium and deuterium reactions we generate the following expression for the KDIE.

$$\frac{k_H}{k_D} = \frac{\frac{k_B T}{h}}{\frac{k_B T}{h}} \frac{\kappa_H}{\kappa_D} \frac{\frac{Q^{\ddagger}_{AHB}}{Q_{AH}Q_B} \exp\left[-\frac{E_{a,H}}{RT}\right]}{\frac{Q^{\ddagger}_{ADB}}{Q_{AD}Q_B} \exp\left[-\frac{E_{a,D}}{RT}\right]} \tag{13}$$

This simplifies to give

$$\frac{k_H}{k_D} = \frac{\kappa_H}{\kappa_D} \frac{Q^{\ddagger}_{AHB}Q_{AD}}{Q^{\ddagger}_{ADB}Q_{AH}} \exp\left[-\frac{[\Delta E_a]^H_D}{RT}\right] \tag{14}$$

The quantity $[\Delta E_a]^H_D$ is merely the difference between the activation energy for the reaction with protium ($E_{a,H}$) and the activation energy for the reaction with deuterium ($E_{a,D}$).

There are essentially two parts to equation 14, each of which may contribute to the magnitude of the KDIE. The first part is the preexponential; it consists of the ratio of the transmission coefficients and the ratio of the partition functions. Under most circumstances both of these ratios are very close to unity. As such they are normally not considered when evaluating KDIEs. However, there are some instances, which will be discussed later, where the observed isotope effects are due almost entirely to the preexponential.

The second portion of equation 14 ($[\Delta E_a]_D^H$) is the zero point energy contribution. The value of $[\Delta E_a]_D^H$, in general, determines the magnitude of most observed isotope effects. In turn, the size of $[\Delta E_a]_D^H$ depends solely on the changes in zero point energy which occur when going from reactants to activated complex.

To understand how $[\Delta E_a]_D^H$ arises we will look back at the hydrogen transfer reaction. As stated earlier, the total zero point energy for a molecule is made up of the contributions from all the vibrational modes of the molecule. More importantly, the zero point energies of the vibrational modes of the protiated and deuteriated molecules are the same except for those vibrations involving the isotopic atom. Therefore, the difference in the total zero point energies between the protiated and deuteriated molecules in the reactants ($[\Delta E_0]_D^H$) and activated complex ($[\Delta E_0^{\ddagger}]_D^H$) is due only to those vibrations involving an isotopic atom.

From Figure 3, which is a more detailed representation of the potential curves for the reactants and activated complex from Figure 2b, it should be fairly clear that if the zero point energy difference in the reactants is the same as the zero point energy difference in the activated complex (i.e., $[\Delta E_0]_D^H = [\Delta E_0^{\ddagger}]_D^H$), then the activation energies for the transfer of protium and the transfer of deuterium should be the same (i.e., $E_{a,H} = E_{a,D}$). If this were the case, then

$[\Delta E_a]_D^H$ would be zero, and consequently there would be no zero point energy contribution to the KDIE. If, however, the zero point energy differences are not the same (i.e., $[\Delta E_0]_D^H \neq [\Delta E_0^{\ddagger}]_D^H$), the activation energies will differ (i.e. $E_{a,H} \neq E_{a,D}$), resulting in a non-zero value for $[\Delta E_a]_D^H$ and a net kinetic isotope effect.

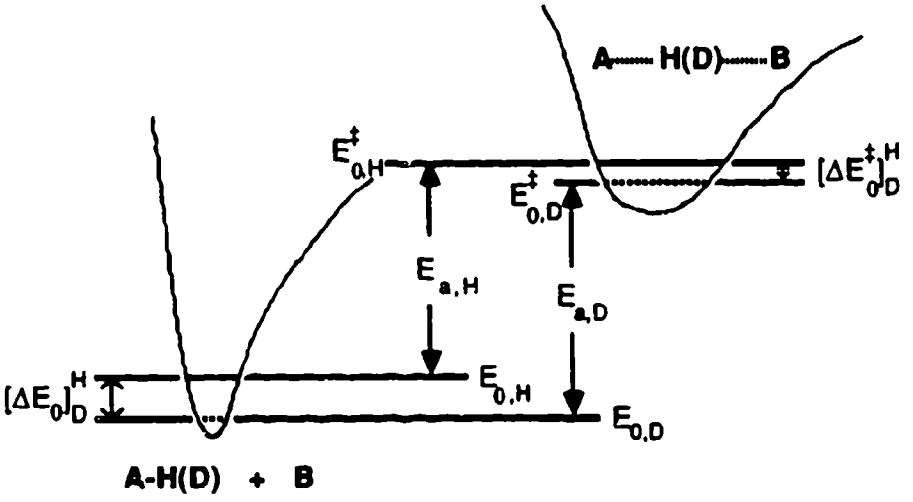

FIGURE 3.[21,36] Potential curves for the the reactants and activated complex.

For $[\Delta E_a]_D^H$ to have a non-zero value, the zero point energy of at least one vibration involving an isotopic atom must change when going from reactants to activated complex. One can see from equation 5 that a change in zero point energy (E_0) requires a change in the vibrational force constant (k).

To illustrate the effect of force constant changes, I will examine a KDIE in a hydrogen transfer reaction (eq. 9) which arises from a change in force constant when the stretching vibration of **A-H** in the ground state becomes the symmetric stretch in the activated complex (i.e., ←**A**····**H**····**B**→). Suppose the force constant for the **A-H** stretch decreases from 465 N/m for the ground state to 116

N/m for the activated complex. This corresponds to lowering the **A-H** frequency from 2800 cm^{-1} to 1400 cm^{-1} (the **A-D** frequency changes form 1979 cm^{-1} to 989 cm^{-1}) for the ground state and activated complex, respectively (the value for the activated complex is the frequency of the hydrogen in the symmetric stretch). For this change in force constant, the zero point energy for the **A-H** stretch decreases from $E_{0,H}$ = 16.74 kJ/mol to $E^{\ddagger}_{0,H}$ = 8.37 kJ/mol, and the zero point energy for the **A-D** stretch decreases from $E_{0,D}$ = 11.80 kJ/mol to $E^{\ddagger}_{0,D}$ = 5.90 kJ/mol. This, in turn, results in a lowering of the zero point energy differences from $[\Delta E_0]^H_D$ = 4.94 kJ/mol for the reactants to $[\Delta E^{\ddagger}_0]^H_D$ = 2.47 kJ/mol for the activated complex. The difference in these two values (note: $[\Delta E_0]^H_D - [\Delta E^{\ddagger}_0]^H_D = [\Delta E_a]^H_D$) gives $[\Delta E_a]^H_D$ = –2.47 kJ/mol. If you place this value into equation 14 and assume the preexponential to be unity, then the resulting KDIE would be 2.7 at 298 K.

From the above example one can see that a decrease in the force constant when going from reactants to activated complex will give a value of k_H/k_D greater than one. Conversely, an increase in the force constant will result in a value of k_H/k_D less than one.

It must pointed out that the above example dealt with only one hydrogen atom, one vibration, and one force constant. In real systems there may be numerous vibrational modes involving isotopic atoms, which undergo changes in their force constants. Each one of these vibrations, in turn, would contribute to the overall magnitude of $[\Delta E_a]^H_D$ and thus contribute to the value of k_H/k_D.

TYPES OF PRIMARY KDIE

KDIEs can be categorized into different types according to the characteristics of their activated complex/transition state. One of the first attempts to classify primary effects was made by Westheimer[26] who

distinguished two different types of linear transition states. More recently Kwart,[26] incorporating Westheimer's categories, classified primary KDIE into four different types. Each of these types will be discussed in detail below.

To diverge momentarily, equation 14 is fine for discussing the theoretical aspects of KDIE. However, it is of limited use when explaining experimental results. Kinetic data are normally obtained from experiments performed at several temperatures. These data are then fitted to the Arrhenius relation

$$k = A \exp\left[-\frac{E_a}{RT}\right] \tag{15}$$

to obtain the activation energy (E_a) and preexponential or frequency factor (A). The Arrhenius equation is an empirical relationship; however, there is some theoretical significance to both E_a and A.[37]

If one performs an operation on equation 15 similar to what was done to generate equation 14, one obtains the following expression for the KDIE.[36]

$$\frac{k_H}{k_D} = \frac{A_H}{A_D} \exp\left[-\frac{[\Delta E_a]_D^H}{RT}\right] \tag{16}$$

This equation is very similar to the relationship for the KDIE derived from transition state theory (eq. 14). In fact, for this level of qualitative discussion it is reasonable to say that the ratio of the Arrhenius preexponentials is approximately equal to the preexponential portion of equation 14.

$$\frac{A_H}{A_D} \approx \frac{\kappa_H}{\kappa_D} \frac{Q^{\ddagger}_{AHB} Q_{AD}}{Q^{\ddagger}_{ADB} Q_{AH}} \tag{17}$$

Because equation 16 is generated from experimental results, it will be used in the following discussion of the four general types of KDIE.

Three out of the four categories of KDIE involve a linear transition state of

the type shown in equation 9 for the transfer of a hydrogen atom from **A** to **B**. The first category involves a linear transition state where the stretching vibration ←**A**····**H**····**B**→ is truly symmetrical.[26] **A** and **B** move in opposite directions while **H** is motionless. Consequently, the frequency and the zero point energy of this symmetric stretch are independent of whether **H** or **D** is present (i.e., $[\Delta E^{\ddagger}_{0}]^{H}_{D} = 0$). A transition state of this type gives a relatively large KDIE because the activation energy difference is equal to the difference in zero point energies for the reactants ($[\Delta E_a]^{H}_{D} = [\Delta E_0]^{H}_{D}$).[36] Assuming a stretching frequency for **A-H** of 3000 cm^{-1}, the value of $[\Delta E_a]^{H}_{D}$ would be –4.65 kJ/mol, and the observed KDIE would be around 6.5 at 298 K. The values of A_H/A_D for the symmetrical activated complex extend over a narrow range from 0.7 to 1.2.[38]

The second category of KDIE involves an unsymmetrical linear transition state.[36] This means that **H**, in the activated complex, is bonded more strongly to either **A** or **B**. Thus, when **A** and **B** move in opposite directions in the "symmetric" stretch (←**A**····**H**····**B**→), **H** will follow the molecule it is bonded to more strongly. Consequently, the frequency and in turn the zero point energy of this so called "symmetric" stretch will depend on whether **H** or **D** is present. As can be seen from the example given in the latter part of the previous section, when there is motion of the isotopic atom in the activated complex $[\Delta E^{\ddagger}_{0}]^{H}_{D} \neq 0$. Because $[\Delta E_0]^{H}_{D} - [\Delta E^{\ddagger}_{0}]^{H}_{D} = [\Delta E_a]^{H}_{D}$, the activation energy differences and consequently the k_H/k_D values will be less than for the truly symmetrical case. In practice, KDIEs attributed to unsymmetrical linear transition states have values between 2 and 5 at 298 K and have values of A_H/A_D between 0.7 and 1.2.[36,38]

A third type of KDIE, possessing a linear transition state, depends on the wave characteristics of the hydrogen atom. The Heisenberg uncertainty principle allows delocalization of a particle across a space corresponding to its deBroglie wavelength.[21,39] If the potential barrier is narrow enough that the

distance between **A** and **B** across the barrier is equal to the deBroglie wavelength of hydrogen, then the hydrogen atom can travel across the barrier to the products side even if its energy is below that of the activated complex. This process is referred to as quantum mechanical tunneling, and it produces kinetic rate constants which are much larger than what is expected by normal transition state theory.[21,32] Because the wavelength of protium is longer than that for deuterium, departures from classical behavior will be greatest for protium. Consequently, KDIEs for reactions involving tunneling are normally quite large; K_H/K_D is often greater than 20.[32] When applying equation 16, which is based on classical transition state theory, to the nonclassical process of tunneling, the values of $[\Delta E_a]_D^H$ will appear to be much less than $[\Delta E_0^{\ddagger}]_D^H$, which in turn results in values of $A_H/A_D << 0.7$.[38]

An alternative to the three types of linear transition states discussed above is a non-linear hydrogen atom transfer, an example of which is shown below.

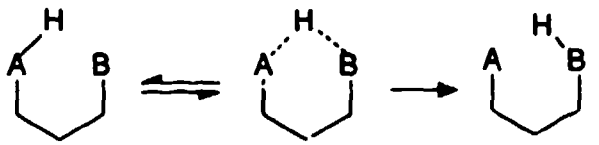

(18)

The non-linear or bent transition state allows relatively free movement of the hydrogen atom. This is in contrast to a linear transition state where the stretching vibrations of the hydrogen atom are limited by the relatively close proximity of molecules **A** and **B**.[36] Stretching vibrations involving **H** change little when moving from reactants to a non-linear transition state. Therefore, the stretching vibrations do not contribute significantly to the value of $[\Delta E_a]_D^H$.

In a non-linear transition state the bending modes of **H** are undergoing the most change. However, since the energies of the bending modes are significantly less than for stretching modes, they too contribute very little to the

value of $[\Delta E_a]_D^H$.[36] Overall, for a bent transition state $[\Delta E_0^{\ddagger}]_D^H$ is almost the same as $[\Delta E_0]_D^H$, thus giving a small value for the difference in activation energies ($[\Delta E_a]_D^H$). Because of the limited contribution from zero point energy, KDIEs for reactions with non-linear transition states are due almost entirely to the preexponential ratio A_H/A_D. Non-linear transition states have KDIE values around 2 at 298 K and can be distinguished from unsymmetrical linear transition states by values of $A_H/A_D > 1.4$.[36]

SECONDARY KDIE

Secondary KDIEs encompass all those isotope effects which do not involve the breaking of a bond to the isotopic atom in the rate limiting step of the reaction. Secondary KDIEs, like primary, arise from changes in vibrational force constants of the normal modes involving the isotopically substituted bonds between the reactants and transition state.[40] In other words, secondary KDIEs are due solely to zero point energy contributions (i.e., $[\Delta E_a]_D^H$).[41,42]

Halevi[43] has classified secondary KDIEs into two different types according to whether or not there is a spatial reorientation of the bond to the isotopic atom when going from reactants to activated complex. Secondary isotope effects of the first kind involve spatial reorientation, whereas secondary isotopes of the second kind do not.

Secondary isotope effects of the first kind have generally been attributed to the rehybridization of the atom the isotope is bonded to.[27,43] This requires that the isotopic atom be alpha to the reaction coordinate (i.e., alpha to the bond breaking).

Streitwieser et al.[44] modeled the secondary KDIE that would occur when a carbon atom rehybridizes from sp^3 to sp^2 as shown in the following reaction

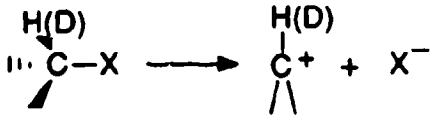

(19)

To calculate the secondary isotope effect, Streitwieser et al. used the following expression derived from transition state theory.

$$\frac{k_H}{k_D} = \prod_i^{\ddagger} \exp\left[\frac{0.1865}{T}\left(\nu_{Hi} - \nu^{\ddagger}_{Hi}\right)\right] \qquad (20)$$

To arrive at this simplified expression, only zero point energy contributions were taken into account, and the approximation $\nu_D = \nu_H/1.35$ was used.

In calculating the secondary isotope effect, Streitwieser et al.[44] looked at changes in the zero point energies of only three vibrational frequencies, one stretching and two bending. To calculate KDIE from equation 20 requires values for vibrational frequencies in both the ground state (ν_{Hi}) and the activated complex ($\nu^{\ddagger}_{Hi}$). Values for the **C-H** stretching and bending frequencies of the ground state sp^3 carbon were easily assigned. However, obtaining the frequencies for the three vibrations in the activated complex required much more effort. Using several different **C-H** vibrations of sp^2 carbon atoms as models, Streitwieser et al. made a best estimate of the values of $\nu^{\ddagger}_{Hi}$.

Figure 4[22,44] shows a breakdown of the contributions of each of the three vibrational modes to the KDIE. The greatest change in frequency occurs when going to the out-of-plane bending vibration in the transition state, and as such this vibration makes the largest contribution to the KDIE. Since equation 18 requires that the product of each vibrational contribution be taken, the resulting value for the KDIE from the data in Figure 4 is 1.48 at 298 K.

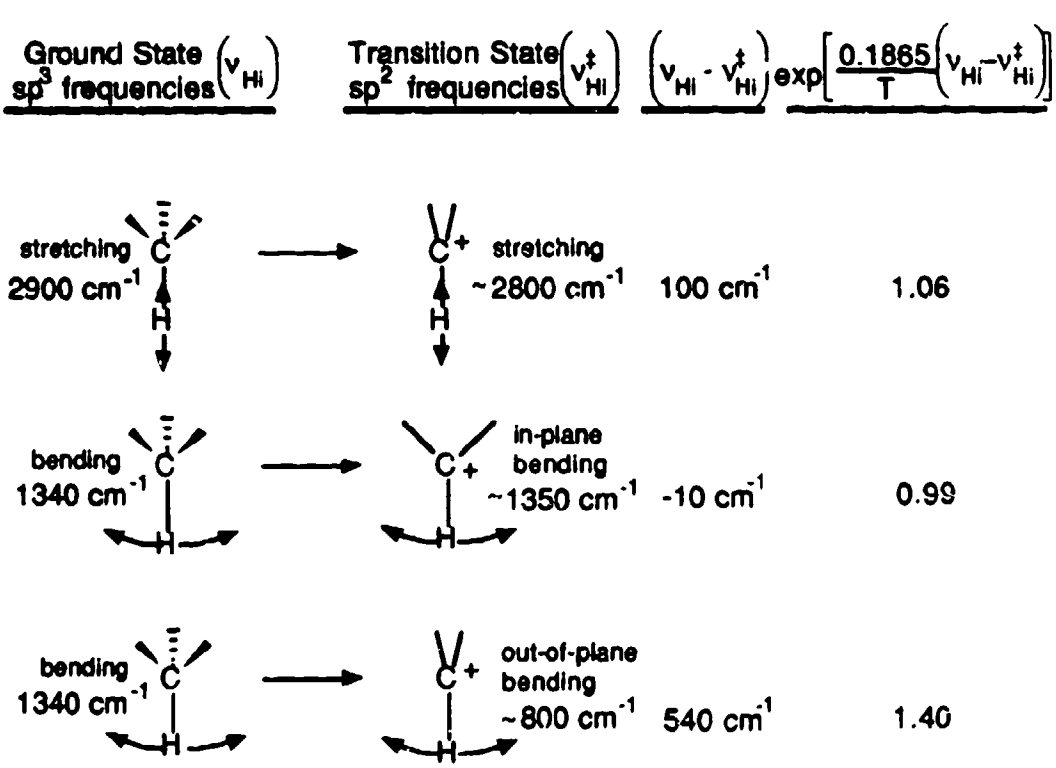

FIGURE 4.[2,24] Calculation of Secondary Isotope Effects at 298 K for Rehybridization of Carbon from sp^3 to sp^2.

Experimentally, values for secondary effects of the first kind are in the range of 1.15 to 1.25 per deuterium at room temperature.[22] For a reaction of the type in equation 19, Streitwieser observed a KDIE of only 1.15.[44] The difference in the experimental (1.15) versus the calculated (1.48) KDIE values above may indicate that the hybridization in the activated complex lies somewhere between sp^3 and sp^2. This would result in a smaller change in the **C-H** bending frequencies when going to the transition state and thus give a smaller KDIE.

Secondary isotope effects of the second kind arise when the isotopic

atom is greater than one bond away from the reaction coordinate (i.e., β, γ, δ). Although there is no spatial reorientation of bonds to the isotopic atom in this type of secondary effect, there are still changes in the force constants of these bonds when going to the activated complex. The cause of secondary isotope effects of the second kind has been much debated.[23,43,44] They have been attributed to hyperconjugation, inductive effects, and steric effects. It seems in most instances that hyperconjugation, which is the interaction of the empty p-orbitals of the carbonium ion with the adjacent carbon-hydrogen σ bond, is the primary cause for this type of secondary effect. This is supported by the fact that in cases of multiple isotopic substitution, such as a β CD_3, there appears to be a conformation dependence of the size of the secondary KDIE. There are instances, however, where both steric and inductive effects may play an important role. The size of secondary isotope effects of the second kind is normally in the range of 1.1 to 1.2 per deuterium at 298 K.[23]

To conclude, secondary KDIEs are small, primarily because frequency changes are small. Bigeleisen and Wolfsberg[22] calculated a secondary isotope effect considering only changes in stretching frequencies. For a decrease in the stretching force constant by a factor of two, they calculated a secondary KDIE for a single deuterium of 1.74. Secondary KDIE values this large are never realized experimentally because the vibrations undergoing the most change in their force constants are bending and not stretching vibrations. Normally, experimental values for secondary KDIEs at room temperature will range from 1.0 to 1.25.

TEMPERATURE DEPENDENCE OF KDIE

The temperature dependence of KDIE may be understood qualitatively by looking back at equation 16. The preexponential ratio (A_H/A_D) can be considered to be relatively temperature independent,[36] whereas the exponential

$(-[\Delta E_a]^H_D/RT)$ is quite obviously temperature dependent. We know from the above discussion that large KDIE (with the exception of tunneling) are due almost entirely to zero point energy contributions. As such KDIE of this type should exhibit a profound dependence on temperature. In contrast, KDIE with only minimal zero point energy contribution should change little with temperature.

The maximum values of $[\Delta E_a]^H_D$ occur for reactions with linear symmetrical transition states.[23,26,27,32] Consequently, KDIEs for this type of reaction will vary the most with temperature. For example, using equation 16 and assuming only zero point energy contributions, a KDIE of 7.0 at 298 K would become a KDIE of 3.4 at 473 K.

For linear unsymmetrical transition states, the values of $[\Delta E_a]^H_D$ are smaller and consequently the temperature dependences of the KDIEs are less than for the symmetrical case. Using equation 16 in the same manner as above, a KDIE for the unsymmetrical case that is 2.0 at 298 K would decrease only to 1.55 at 473 K.

Non-linear transition states have values of $[\Delta E_a]^H_D$ that are very close to zero. As such, the preexponential A_H/A_D is the primary source of the KDIE for reactions of this type. Because A_H/A_D varies little with temperature, KDIEs for reactions with non-linear transition states tend to be temperature independent. In fact a constant KDIE over temperature ranges greater than 50 degrees is a strong indication of a bent transition state.[36]

When the extrapolation of KDIE is carried out to extremely high temperatures the exponential portion of equation 14 reduces to unity. This leaves only the preexponential A_H/A_D to contribute to the KDIE. What this preexponential actually represents is the ratio of partition functions (eq. 17) which at high temperature reduce to $\nu^{\ddagger}_{HL}/\nu^{\ddagger}_{DL}$, the ratio of imaginary frequencies

describing the motion along the reaction coordinate.[22,32] At infinite temperature the value of this ratio of imaginary frequencies and thus the value of the KDIE should in theory fall between unity and $(\mu^{\ddagger}_{DL}/\mu^{\ddagger}_{HL})^{1/2}$ (the ratio of the reduced masses along the reaction path).[32]

For primary KDIEs, where the isotopic atom is in motion along the reaction path, the infinite mass approximation (see equations 6, 7, and 8) can be used to give

$$\sqrt{\frac{\mu^{\ddagger}_{DL}}{\mu^{\ddagger}_{HL}}} = \sqrt{\frac{m_D}{m_H}} \qquad (21)$$

where m is the mass of the isotopic atom. Thus, the high temperature limiting value for a primary KDIE should be $(2)^{1/2}$ or 1.41. However, due to anharmonicities and inaccuracies in the infinite mass approximation this value is closer to 1.35.[44]

In secondary KDIEs, the isotopic atom is not involved in motion along the reaction path. As such the infinite mass approximation cannot be used to simplify the ratio of reduced masses $(\mu^{\ddagger}_{DL}/\mu^{\ddagger}_{HL})^{1/2}$. Because of the small size of the isotopic atom and its rather minor contribution to the reduced mass, $\mu^{\ddagger}_{DL}$ is only slightly larger than $\mu^{\ddagger}_{HL}$, giving a value of $(\mu^{\ddagger}_{DL}/\mu^{\ddagger}_{HL})^{1/2}$ very close to unity. Thus, at infinite temperature, secondary KDIEs approach unity.

The above discussion of temperature dependence is an oversimplification of a very complex subject. Temperature dependence is not as straightforward as the above discussion would indicate. However, in general, one can conclude that the larger the value of $[\Delta E_a]^H_D$ for a particular reaction the more the KDIE for that reaction will change with changes in temperature.

CONCLUSIONS

In the discussions thus far, I have tried to focus my attentions on the KDIE

arising from a single isotopic atom. It is frequently the case, however, that reactions are performed on molecules containing more that one isotopic atom. This gives rise to the possibility of compounded isotope effects. Essentially, when there is more than one isotopic atom, the effects of each atom multiply.[23] This of course assumes that there is only one isotopic atom contributing a primary effect and the remaining atoms contribute secondary effects or that all isotopic atoms contribute secondary effects.

In looking back at the calculation of the secondary KDIE performed by Streitwieser et al.,[44] suppose instead of using one isotopic atom they had used three. The resulting calculations would involve three frequencies from each isotopic atom. The resulting KDIE would be the product of the contributions of all nine frequencies, or in other words the product of the isotope effects for each of the three atoms. If the isotope effect of each atom were the same as the secondary isotope effect for the single atom case (i.e., 1.48), then the resulting KDIE would be $(1.48)^3$ or 3.24.

The compounding of isotope effects is not limited to secondary effects. It is quite possible to have a compounded isotope effect where one atom contributes a primary effect and one or more atoms contribute a secondary effect.

The presence of multiple isotopic substitution also complicates the temperature dependence of observed KDIE. Because the effects of the various isotopic atoms may exhibit different degrees of temperature dependence, the net temperature dependence of the observed KDIE may be quite complex.

The determination of whether an isotope effect is primary or secondary is relatively straightforward for reactions involving a single isotopic atom. If the observed effect is greater than the maximum possible secondary effect, then the KDIE can unambiguously be assigned to a primary effect. If however, the KDIE

is less than the maximum secondary effect, then other information must be used to determine whether the effect is primary or secondary.

The evaluation of KDIE becomes an order of magnitude more complex when multiple isotopic substitution is involved. Because of the possibility of large compounded secondary effects, only the largest KDIE can be confidently assigned as primary. For smaller isotope effects it may be possible to make clear assignments only if information from other types of experiments is used.

CRITICAL EVALUATION OF ENERGETIC MATERIAL KDIE STUDIES

OVERVIEW

Because of the complexity of KDIE theory, approximations have been made in an effort to simplify its application to experimental data. Unfortunately, KDIE theory has frequently been oversimplified to the point where it becomes valid only under idealized circumstances. The resulting application of this simplified model to experimental data has led to frequent errors in the interpretation of KDIE. [26]

The KDIE studies of energetic materials epitomize the problems in interpretation which have plagued isotope effect studies since their inception. Publications in this area have utilized 1.41[45] (1.35 in more recent papers)[19] as a dividing line between primary and secondary isotope effects. In these studies, experimental KDIE values were generally designated as primary if they were greater than 1.41 (1.35) and as secondary if they were less than 1.41 (1.35). This number is essentially empirical in nature and possesses only limited theoretical significance with respect to whether an effect is primary or secondary. Its only importance in KDIE theory stems from the fact that at infinite temperature the maximum possible primary effect is approximately 1.35.[32,44] It is quite possible to have compounded secondary effects greater than 1.41(1.35), and it is also altogether possible to have primary effects less than 1.41(1.35).

Fortuitously, the 1.41(1.35) dividing line lies within the range of what can

be expected for a primary effect in the thermal processes of energetic materials. As we shall see in the following discussion, when more rigorous guidelines are applied to the energetic material KDIE data the assignments made using the 1.41(1.35) criterion appear in most cases to be correct.

The application of KDIE to the study of energetic materials has been at best a difficult proposition. In addition to the problems associated with the oversimplification of KDIE theory, there are other obstacles to obtaining and interpreting isotope effect data. The thermal processes of energetic materials (decomposition, pyrolysis, combustion, and detonation) are quite complex. Their mechanisms consist of numerous steps and may involve several parallel pathways each with its own rate limiting process. The precision of the techniques used to study these thermal processes tends to be poor, which in turn leads to KDIE values with relatively large uncertainties. Often kinetic rate constants cannot be measured directly; as a result, ratios of other parameters, which are hopefully related to the rate constant, must be used to obtain isotope effect values. Finally, the very nature of these processes necessitates that experiments be performed at relatively high temperatures (473 to 673K). As a consequence of this and other factors, KDIE values obtained for the thermal processes of energetic materials are small.

TRINITROTOLUENE

Shackelford et al.[45] were the first to apply the technique of KDIE to the study of energetic materials. They attempted to elucidate the rate limiting process in the thermal decomposition of liquid 2,4,6-trinitrotoluene (TNT). Like most energetic organic compounds, TNT exhibits autocatalytic behavior upon decomposition.[46,47] However, unlike the nitramines to be discussed later, TNT produces relatively few gaseous products during decomposition.[48] The

decomposition of TNT proceeds initially through a long induction period characterized by minimal heat evolution. During the induction phase a catalytic species is generated which at a certain threshold concentration initiates an exothermic acceleratory phase. The acceleratory phase is followed, after the point of maximum heat release, by a decay phase which continues until decomposition is complete.[45,46]

Using isothermal differential scanning calorimetry (IDSC), Shackelford et al.[45] obtained data for the decomposition of TNT and its α,α,α-trideuteriomethyl analogue (TNT-d_3) at temperatures ranging from 518 to 542 K. Applying first order kinetics to the data for the decay phase, they obtained rate constants for both TNT and TNT-d_3. The average value for k_H/k_D for the temperature range studied was given as 1.35 ± 0.02. However, using the rate constant data they supplied for each temperature, I obtained an average KDIE for the decay phase of 1.38 ± 0.20 at the 95% confidence level. No explanation can be offered for the disparity in the manipulation of their data. (When the decay phase KDIE is discussed in the text below, both isotope effect values will be given.)

Rate constants could not be obtained for the induction phase of TNT decomposition. However, it was suggested that the induction time, which is the time between the beginning of the DSC experiment and the onset of the acceleratory phase, should be inversely proportional to the rate constant such that

$$\frac{k_H}{k_D} = \frac{t_{ID}}{t_{IH}} \qquad (22)$$

where t_{ID} is the induction time for TNT-d_3 and t_{IH} is the induction time for TNT. Using equation 19, an average isotope effect for the induction phase of 1.66 ± 0.20 was obtained.[45]

Shackelford et al., using 1.41 as the dividing line between primary and

secondary KDIE, stated that the induction phase KDIE of 1.66 was clearly a primary isotope effect. Although less than 1.41, they attributed the decay phase isotope effect of 1.35 (1.38) to a diluted primary isotope effect.

The following chemical evidence was used to support the above assignments. Data obtained by Dacons et al.[48] and Rogers[49] indicated that the initial decomposition of TNT proceeds via the oxidation of the methyl moiety. Depending on reaction conditions the oxidation of TNT may proceed from

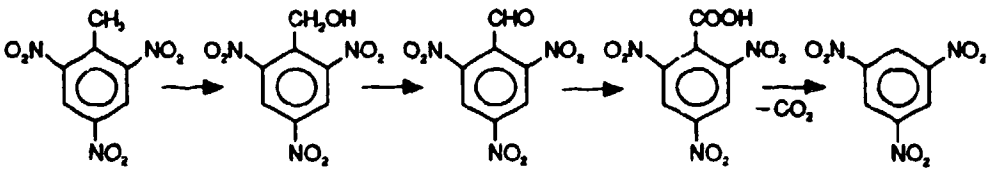

TNT 1 2 3 4 (23)

2,4,6-trinitrobenzyl alcohol (**1**) through 2,4,6-trinitrobenzyaldehyde (**2**) to form 2,4,6-trinitrobenzoic acid (**3**) which then readily decarboxylates to give 2,4,6-trinitrobenzene (**4**) (eq. 23), or equation 23 may be followed through the production of **2** which then reacts with other species in the liquid TNT to produce a myriad of decomposition products called "explosive coke."[48,49] The formation of **1**, **2**, and **3** requires the rupture of C-H bonds. Although the decarboxylation of **3** necessitates a C-C bond rupture, the absence of α-hydrogens precludes any significant KDIE.

When small amounts of hydroquinone, which possesses a labile hydroxyl hydrogen,[45] were introduced into liquid TNT a significant decrease in the induction time was observed. These results appear to require some type of bimolecular hydrogen transfer between hydroquinone and TNT, and thus imply that the rate controlling process during the induction phase (and presumably during the entire decomposition) involves a hydrogen transfer between two TNT

molecules (i.e., a C-H bond rupture). However, one cannot entirely rule out the possibility that the hydroquinone accelerates a radical process not involving a C-H bond rupture.

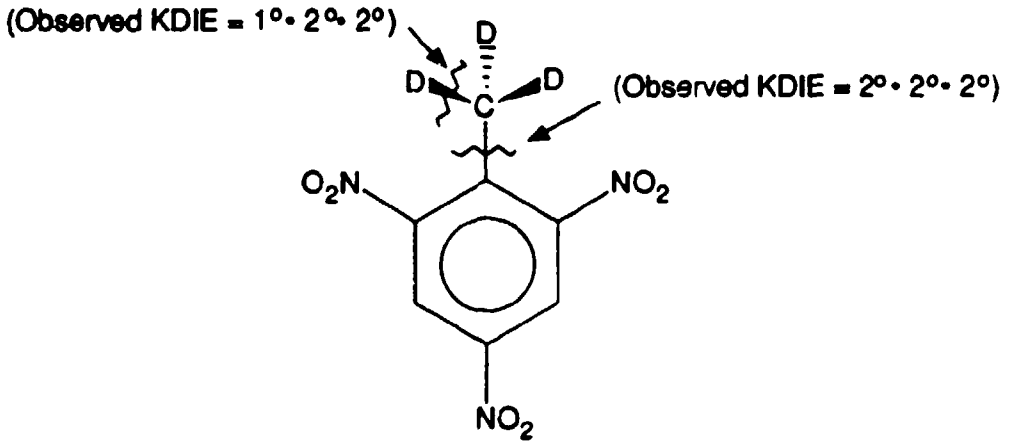

FIGURE 5. Possible Isotope Effects in TNT-d_3

For a TNT molecule with deuterium substitution at the methyl moiety, an isotope effect should be observed if either a methyl carbon-hydrogen bond or the benzylic carbon-carbon bond were broken in the rate determining step. In the case of a C-H bond rupture there would be two secondary effects, due to the two remaining deuteriums on the methyl carbon, in addition to the obvious primary effect (Fig. 5). The observed isotope effect would be the product of a primary effect compounded by two secondary effects (i.e., 1° • 2° • 2°). As shown in Figure 5, the observed isotope effect for a C-C bond rupture would simply be the product of the secondary effects resulting from the three methyl deuteriums (i.e., 2° • 2° • 2°).

The TNT decomposition KDIE of 1.35 (1.38) and 1.66 are very small for compounded primary effects when considering that they are the product of the

isotope effects from three deuterium atoms. Room temperature compounded secondary effects have been known to have values larger than the KDIE observed for TNT.[23,27,40,43] Consequently, even with chemical evidence supplied by Shackelford et al., the absolute assignment of the TNT KDIE as primary is somewhat tenuous.

Fortunately, the evaluation of the KDIE in TNT decomposition has been significantly clarified by additional research in this area. Bulusu and coworkers[18,50] qualitatively confirmed the work of Shackelford et al.[45] by observing isotope effects in both the decomposition and detonation of TNT. More importantly, recent electron paramagnetic resonance (EPR) studies[51] indicate that the transition state for TNT decomposition involves a bimolecular hydrogen atom transfer between the methyl moiety of one TNT molecule and the para nitro- group of a second TNT molecule (Fig. 6). The EPR results, which are in agreement with the previous hydroquinone experiments, provide reasonably conclusive proof that a C-H bond rupture is indeed the rate controlling process in TNT decomposition.

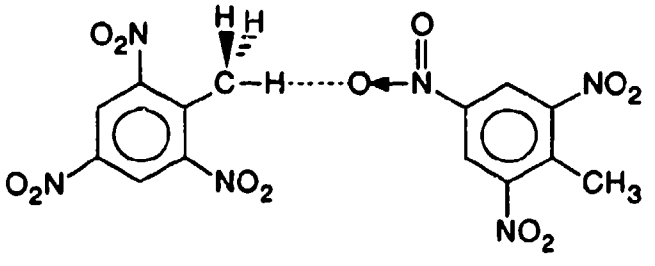

FIGURE 6. Possible Bimolecular TNT Transition State.

Interestingly, the ratio of preexponentials (A_H/A_D) for the decay phase of TNT decomposition is approximately one. Assuming the decay phase KDIE is temperature dependent, then following Kwart's[36] criteria, the decomposition

should proceed through a linear unsymmetrical transition state, as is indicated by EPR. Unfortunately, little weight can be given to this observation because of the large uncertainties and undefined temperature dependence of the TNT isotope effect.

Since we can say with some confidence that the 1.35 (1.38) and 1.66 values are compounded primary effects, it is possible to make estimates of the magnitude of the primary and secondary contributions to these effects. The thermolysis of 4-methylene-1-pyrozolines shows an average secondary effect of 1.07 to 1.08 per α-deuterium at 443 K.[52] Assuming this reaction to have a similar transition state to that of TNT decomposition, a reasonable estimate for the secondary effect would be 1.07 per deuterium.

In the few studies for which both primary and secondary effects were independently measured for the same reaction, the primary isotope effect was always significantly larger than the secondary isotope effect.[23,52] For example, Reference 23 gives independently measured primary and secondary isotope effects for an elimination reaction at 323 K of 2.98 and 1.30, respectively. Assuming a similar relationship between the primary and secondary effects for TNT decomposition and that the secondary effect for TNT is approximately 1.07, a corresponding primary effect can be calculated by a temperature extrapolation. This is accomplished by first using equation 16 and treating the preexponential ratios as one; the KDIE of 1.30 at 298 K is extrapolated to the temperature at which it decreases to 1.07. The KDIE of 2.98 at 298 K is then extrapolated to this same temperature, giving a value of 1.32. Thus, the estimated primary and secondary isotope effects for TNT decomposition (518 to 542 K) per deuterium are 1.32 and 1.07, respectively. Using these estimates, one would obtain a value for the compounded primary effect in TNT decomposition of 1.51 (i.e. 1.32 • 1.07 • 1.07), which is in reasonable agreement

with both the observed KDIE values.

It must be pointed out that by simply assuming the TNT secondary effect to be 1.07 and then determining what magnitude of primary effect would give the observed KDIE values, a value of approximately 1.32 for the primary effect would be obtained.

The magnitude of the contribution of a deuterium atom to an observed KDIE will certainly depend on the configuration of the transition state and clearly reactions involving different compounds will have different transition states. However, there are some similarities between the thermal reactions of nitroaromatics and nitramines. Although crude, the TNT KDIE values of 1.32 for a primary contribution and 1.07 for a secondary contribution provide the only reasonable estimate for isotope effect values in the thermal processes of energetic materials at elevated temperatures. Consequently, these values will be used to help evaluate KDIEs in the following discussions.

TRIAMINOTRINITROBENZENE

Rogers et al.[53] extended the isotope effect studies of energetic materials to the solid state decomposition of 1,3,5-triamino-2,4,6-trinitrobenzene (TATB). Performing IDSC experiments on TATB and TATB-d_3 similar to those done for TNT over a temperature range of 570-655 K, they obtained a value for k_H/k_D of approximately 1.5. Using the 1.41 criterion,[45] they attributed this to a primary effect.

Because of the lack of information given in their paper it is difficult to assess the validity of the conclusions made by Rogers et al.[53] The isotope effect in TATB is due to changes in the force constants of N-H bonds, as opposed to C-H bonds in the case of TNT. N-H stretching frequencies are slightly larger than the corresponding C-H frequencies,[54] so one would expect the isotope

effects for N-H bonds in general to be somewhat larger than those for C-H bonds. However, due to the fact that the TATB decomposition occurs approximately 100 degrees higher the TNT decomposition, our reference values of 1.32 for primary and 1.07 for secondary should still be approximately valid. This of course assumes that the TATB KDIE decreases with increasing temperature. Thus, if the numerous approximations are reasonable, then a primary KDIE in TATB decomposition should be around 1.41 (i.e., $1^{o} \cdot 2^{o} = 1.32 \cdot 1.07$). Considering the precision of IDSC data and the approximations made, this is in relatively good agreement with experiment.

The results of Rogers et al.[54] are important in that they were the first to demonstrate a significant isotope effect in the solid state. The solid state TATB experiments differ from the liquid TNT experiments in that the TATB is much more restricted in its motions and thus more limited in the possible transition state configurations it can assume, due to the strong intermolecular forces in the solid state. Therefore, it is somewhat surprising that a KDIE of this magnitude was observed for TATB decomposition.

HMX AND RDX

Recently, KDIE have been used to study the rate limiting processes in the decomposition,[17-20] deflagration,[19] and combustion[16,17,55] of HMX and RDX. The evaluation of the isotope effects and assignment of the rate limiting processes for these thermal events was made using almost exclusively the empirical criteria of Shackelford et al. (i.e. 1.35).[19] Unlike the TNT case, however, there is lack of clear experimental evidence to corroborate the determinations made from the isotope effect data. Consequently, conclusions made from KDIEs, which will be discussed below, must be treated with care until other methods can be found to verify these results.

HMX and RDX are cyclic nitramines which differ by only one methylene nitramine unit. Consequently, the possible isotope effects for HMX and RDX are almost identical. For deuterium substitution at the methylene carbons, isotope effects should be observed if either a C-H, C-N, or N-N bond were broken in the rate limiting process. A C-H bond rupture would result in a compounded primary effect due to a primary contribution from the deuterium in motion along the reaction path and a secondary contribution from the deuterium alpha to the reaction path (Fig. 7). Using the TNT-based values, the estimated magnitude for a KDIE from a C-H bond rupture would be 1.32 • 1.07 = 1.41 (by sheer coincidence this happens to be the same as the empirical value originated by Shackelford et al.[45]). In theory, the four deuteriums gamma to the reaction path could contribute to the compounded primary effect. However, considering the small size of α-secondary effects under these conditions, it should be reasonable to neglect the secondary effects of the γ-deuteriums.

A C-N bond rupture in the rate limiting process would result in a compounded secondary effect made up of the contributions from the two α-deuteriums and the two β-deuteriums (Fig. 7). Depending on the orientation of the activated complex, the isotopic effects of β-deuteriums (secondary isotope effects of the second kind) can be as large as the effects of α-deuteriums (secondary isotope effects of the first kind). Under most conditions, however, the effects of β-deuteriums are smaller. Assuming this to be the case, an acceptable estimate for the contribution of the β-deuteriums to the compounded secondary KDIE would be 1.02 per deuterium.[23,40,43] Using this approximation and the TNT based values, the estimated magnitude for the effect for a C-N bond rupture would be 1.07 • 1.07 • 1.02 • 1.02 = 1.19. For this estimate I have chosen to neglect the possible contributions of deuteriums gamma and delta to the reaction path.

There is sufficient evidence both theoretical[76] and experimental[15,19,20] to conclude that the N-N bond is the weakest covalent bond in HMX and RDX. Furthermore, these studies indicate that the N-N bond rupture is relatively facile at the temperatures of nitramine decomposition.[56] Consequently, it was concluded that the N-N bond rupture was unlikely to be the rate limiting process. For the sake of this research we will assume this conclusion to be correct.

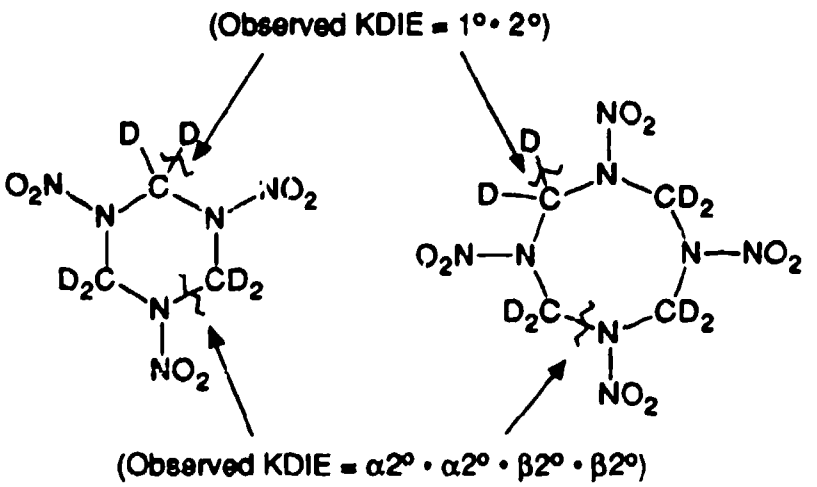

FIGURE 7. Possible Isotope Effects in RDX-d_6 and HMX-d_8.

KDIE in HMX Decomposition

HMX decomposition, as measured by IDSC, possesses three phases similar to what is seen in TNT decomposition. Shackelford et al.[19] attributed the induction phase, the exothermic acceleratory phase, and the decay phase to physical states of HMX: solid, mixed melt, and liquid, respectively. The KDIEs for each of these phases are listed in Table I.

There are two KDIE values listed for each phase of HMX decomposition.

The values given for HMX and HMX-d_8 prepared under different conditions have to be questioned somewhat because it is not known how much of the rate differences are due to differences in sample history. Therefore, the KDIE values for the identically prepared HMX and HMX-d_8 should be given more credence even though they represent a narrower temperature range and smaller number of replicate measurements.

TABLE I

Deuterium Isotope Effects in HMX Decomposition

Method	Temp. Range (K)	Physical State	Ratio	KDIE	Ref.
IDSC	551-553	solid	$t_{1/2D}/t_{1/2H}$	2.21 ± 0.18[a]	19
IDSC	551	solid	$t_{1/2D}/t_{1/2H}$	1.74 ± 0.22[b]	19
IDSC	551-553	mixed melt	K_H/K_D	0.85 ± 0.22[a]	19
IDSC	551	mixed melt	K_H/K_D	1.05 ± 0.18[b]	19
IDSC	551-553	liquid	K_H/K_D	1.13 ± 0.08[a]	19
IDSC	551	liquid	K_H/K_D	1.28 ± 0.21[b]	19
TGA	508-555	solid and melt	K_H/K_D	2.07± 0.11[a]	20
TGA	508-555	solid and melt	$t_{1/2D}/t_{1/2H}$	1.91± 0.17[a]	20

[a] HMX and HMX-d_8 were prepared by different methods. [b] HMX and HMX-d_8 were prepared by identical methods.

Shackelford et al.,[19] using their empirical criteria, attributed the induction phase KDIEs, 2.21 ± 0.18 and 1.74 ± 0.22, to a rate controlling C-H bond rupture. To determine whether these values are indeed due to a compounded primary effect, one needs to look at what it would take for these values to be the result of a compounded secondary effect. Compounded secondary effects have

been known to be larger than these values but not at the temperatures of HMX decomposition. Even if one assumed that the secondary effects for the β-deuteriums were as large as those for the α-deuteriums (i.e., 1.07), one would still obtain only a compounded secondary effect of $(1.07)^4$ or 1.31, which is far below the observed value. To arrive at a compounded secondary effect in the range of 1.74 would require, for example, effects of 1.20 for each α-deuterium and 1.10 for each β-deuterium. While not impossible, secondary effects of these magnitudes are unlikely at the elevated temperatures of HMX decomposition. Therefore by default, it would seem that the assessment of a rate controlling C-H bond rupture is reasonable.

The values given for the KDIE in the mixed melt were 0.85 ± 0.22 for the HMX and HMX-d_8 prepared by different methods and 1.05 ± 0.18 for the identically synthesized. Shackelford et al.,[19] placing more significance on the 0.85 value, stated that the mixed melt exhibited an inverse isotope effect which they attributed to differences in C-H and C-D bond contractions during liquefaction. Because their explanation places a great deal of significance on the physical state of the HMX, it would seem that the value for the identically synthesized HMX and HMX-d_8 would be a more valid measure of this type of isotope effect. The rate differences giving this "inverse" isotope effect of 0.85 are likely the result of differences in impurities, crystal size, defects, etc. between the HMX and HMX-d_8 and not the result of deuterium substitution. Given the conflicting data and the large uncertainties in both KDIEs for the mixed melt, the no conclusive evidence of a KDIE in the mixed melt, inverse or normal.

The KDIE values for the liquid HMX (1.13 ± 0.08 and 1.28 ± 0.21) were attributed by Shackelford et al. to a rate controlling C-N bond rupture. However, isotope effects of these magnitudes could quite possibly be either compounded

primary or compounded secondary effects. Without other information it is impossible to confirm their assignment.

Bulusu et al.[20] employed thermogravimetric analysis (TGA) to study isotope effects in HMX decomposition. Because nitramine decomposition proceeds to gaseous products early on, thermogravimetric analysis, which measures sample weight loss with time, is a viable method for measuring rate constants and thus isotope effects. The KDIE values obtained for HMX decomposition using TGA are listed in Table I. Interestingly, Bulusu et al. did not observe the complex decomposition behavior that was seen in IDSC experiments. They obtained essentially one KDIE for the entire decomposition experiment (2.07 ± 0.11 determined from the ratio of rates and 1.9 ± 0.17 determined from the ratio of induction times). Using the empirical 1.35 criterion,[19] Bulusu et al. attributed the isotope effect to a rate limiting C-H bond rupture. Following the logic used to explain the KDIE in the IDSC induction phase, the isotope effects measured by TGA by default appear to be a primary effect compounded by secondary effects.

One interesting observation made by Bulusu et al.[20] was the apparent temperature independence of the HMX KDIE over a temperature range of 508-555 K. From this observation they attempted to invoke Kwart's[36] criteria to suggest that the HMX decomposition went by a non-linear transition state. This observation, however, is little more than conjecture. Data an order of magnitude more precise than what is obtained from either the TGA or IDSC experiments would be necessary before any justifiable conclusions about the configuration of the transition state in HMX decomposition could be made.

KDIE in RDX Decomposition

The KDIE values obtained for RDX decomposition are given in Table II.

The isotope effect values for IDSC and TGA are in the same range even though the TGA measured the KDIE for the solid state decomposition while IDSC measured KDIE for decomposition in the liquid. Using the 1.35 criterion,[19] all three KDIE for RDX decomposition were designated as primary.[17,20] Although the TGA value of 1.50 is smaller than the IDSC values, it would still require a relatively large secondary effect from all four deuteriums for it to be the result of a compounded secondary effect. Therefore, as was the case of the HMX induction phase because it seems unlikely that the effects can be due to a compounded secondary effect, the KDIE for RDX decomposition appears to be the result of a rate controlling C-H bond rupture.

TABLE II

Deuterium Isotope Effects in RDX Decomposition

Method	Temp. Range (K)	Physical State	Ratio	KDIE	Ref.
IDSC	505	liquid	K_H/K_D	2.06± 1.07[a,b]	17
IDSC	510	liquid	K_H/K_D	1.74 ± 0.17[b]	17
TGA	472-489	solid	K_H/K_D	1.50 ± 0.06[c]	20

[a] This is a preliminary value based on six measurements each for RDX and RDX-d_6. [b] The RDX and RDX-d_6 were prepared by identical methods. [c] The RDX and RDX-d_6 were prepared by different methods.

KDIE in HMX and RDX Combustion

The burn rates of pressed pellets of HMX and HMX-d_8 were measured at three different pressures. The ratio of the burn rates (r_H/r_D), which was assumed to be equivalent to the ratio of rate constants, at each pressure are given in Table III. Shackelford et al.,[16] using the 1.35 dividing line, designated the 1.37

± 0.24 and 1.61 ± 0.11 at 500 and 1000 psig respectively as primary effects. The value at 1500 psig of 1.24 ± 0.13 was assigned to a secondary effect.

HMX combustion normally proceeds through an exothermic decomposition producing gaseous products which further react in the flame. The change in the isotope effect with pressure was attributed to a change in the physical state where a majority of the HMX decomposition occurred. Shackelford et al.[16] speculated that as pressure increased, the HMX decomposition went from the solid state to the liquid. While their explanation for the variation in KDIE values is possible, it is much more likely that the differences between pressures are simply due to statistical fluctuations.[57] If this is correct, then a more reasonable value for the isotope effects in HMX combustion would be an average of the KDIE for all three pressures (i.e., 1.40 ± 0.11).

TABLE III

Deuterium Isotope Effects in HMX and RDX Combustion

Compound	Pressure (psig)	KDIE (r_H/r_D)	Ref.
HMX	500	1.37 ± 0.24	16
HMX	1000	1.61 ± 0.11	16
HMX	1500	1.24 ± 0.13	16
RDX	500	1.37 ± 0.16	17
RDX	1000	1.46 ± 0.23	17

The burn rates of pressed pellets of RDX and RDX-d_6 were also measured at 500 and 1000 psig. The ratio of these burn rates at each pressure is listed in Table III. Shackelford et al.,[17] using the same logic applied to HMX, designated these effects as primary.

The isotope effects in HMX and RDX combustion are larger than the estimated magnitude for the compounded effect resulting from a C-N bond rupture. However, given the uncertainties in both the KDIE values and the compounded secondary estimate, this is far from conclusive proof that the combustion isotope effects are the result of a C-H bond rupture in the rate limiting step.

If one assumes that the rate of decomposition of HMX and RDX in the condensed phase controls the rate of combustion, then the KDIE results for decomposition can be used to help interpret the isotope effects for HMX and RDX combustion. The average HMX KDIE of 1.40 ± 0.11 and the average RDX KDIE of 1.42 ± 0.15 are smaller than the compounded primary isotope effects in HMX and RDX decomposition. Much of this difference may simply be due to the fact that the temperature of the burning surface, where nitramine decomposition takes place, is approximately 100 to 200 degrees higher than the temperatures studied for HMX and RDX decomposition. Assuming even a small temperature dependence of the KDIE for HMX and RDX decomposition, a change in temperature of this magnitude could account for the differences in isotope effect values between decomposition and combustion. If this is truly the case, then it would indicate that the KDIEs for HMX and RDX combustion are more than likely the result of a rate controlling C-H bond rupture.

The true relationship between burn rate and the kinetic rate constant of the slowest step has yet to be clearly addressed. Shackelford and coworkers[16,17] simply assumed the two quantities were proportional to each

other. While reasonable, this assumption needs to be investigated in more detail.

CONCLUSIONS

The poor precision of the KDIE for the decomposition and combustion of the nitramines (HMX and RDX) and the lack of other chemical evidence would make many chemists shy away from making many conclusions concerning the possible rate limiting process. One must understand the difficulties associated with these types of experiments and accept the above data as the best available at the present time. One can say with confidence that the isotope effects are real. However, to go beyond this requires that the assumptions and approximations made in the above discussion be valid. If they are, then it would appear that under most circumstances, a C-H bond rupture is the rate controlling process in HMX and RDX decomposition and combustion.

EXPERIMENTAL

SYNTHESIZED COMPOUNDS

This experimental section describes the synthesis of HMX, RDX, and their fully deuteriated analogs HMX-d_8 and RDX-d_6. The synthesis of HMX and RDX are described in varying degrees of detail in the literature.[16,19,58-62] However, for the sake of completeness and at the risk of repeating information already contained in the literature, I will endeavor to give a full account of the synthesis of HMX, HMX-d_8, RDX, RDX-d_6.

To ensure that differences in experimental results were not due to impurities or sample history, the deuteriated forms of HMX and RDX were synthesized in the same manner as the protiated forms. This was accomplished by simply substituting paraformaldehyde-d_2 for paraformaldehyde in the synthesis of hexamethylenetetramine to give hexamethylenetetramine-d_{12}. The deuteriated hexamethylenetetramine was then used in the synthesis of either HMX-d_8 or RDX-d_6.

All chemicals were reagent grade or better and were used without purification. The paraformaldehyde-d_2 was obtained from MSD Isotopes. Burdick and Jackson distilled-in-glass acetone was used to convert HMX from the α- to the β-polymorph. A JEOL FX-90Q 90MHz FT-NMR was used to obtain all ^1H spectra. Melting point data were obtained using a Thomas-Hoover Unimelt capillary melting apparatus and unsealed capillary tubes. All melting points are uncorrected. An Olympus model AHMT optical microscope was used

to obtain optical micrographs of the α and β forms of HMX.

Synthesis of Anhydrous HNO_3

Because 98-100% nitric acid is an essential reagent in the final nitration steps of both HMX and RDX, it is first necessary to describe its preparation.[63] Concentrated sulfuric acid (1000 mL) was added to a two-liter three-neck round-bottom flask. The sulfuric acid was cooled in a dry ice/acetone bath as 600 g (5.95 mol) of KNO_3 was slowly added with stirring from an overhead mechanical stirrer. Upon complete dissolution of the potassium nitrate, the mechanical stirrer was removed, and a still head, thermometer, condenser, bent adapter, and 500-mL round-bottom flask were attached in preparation for vacuum distillation. The 500-mL collection flask was placed in a dry ice/acetone bath, and a methanol-ethylene glycol mixture cooled to –30 °C was circulated through the condenser. The apparatus was then slowly evacuated to a pressure of 46–47 torr. The reaction flask was allowed gradually to warm to room temperature as the HNO_3 distilled off. After HNO_3 bubble evolution slowed, the solution was slowly heated to 60 °C. The distillation was stopped as soon as any evidence of red NO_2 was observed. Normally this was seen as a slight yellow tint to the condensate in the apparatus. The frozen HNO_3 was allowed to liquefy slowly in a refrigerator. The clear liquid HNO_3 was then transferred to Teflon bottles under a nitrogen atmosphere and stored in a refrigerator to prevent decomposition.

Yield 362 g (97%).

CAUTION: HMX and RDX are both high explosives and as such great care must be exercised at all times during the synthesis of these compounds. HMX is 1.6 times more powerful than TNT and is second only to hexanitrobenzene in

explosive force. Teflon (not Teflon coated) utensils must be used in place of metal utensils during synthesis to preclude accidental spark ignition. In addition, all glassware should be cleaned thoroughly and be free of scratches.

Synthesis of HMX

The synthesis of HMX and HMX-d_8 follows a four step procedure diagramed in Figure 8 and outlined in detail in the text below.

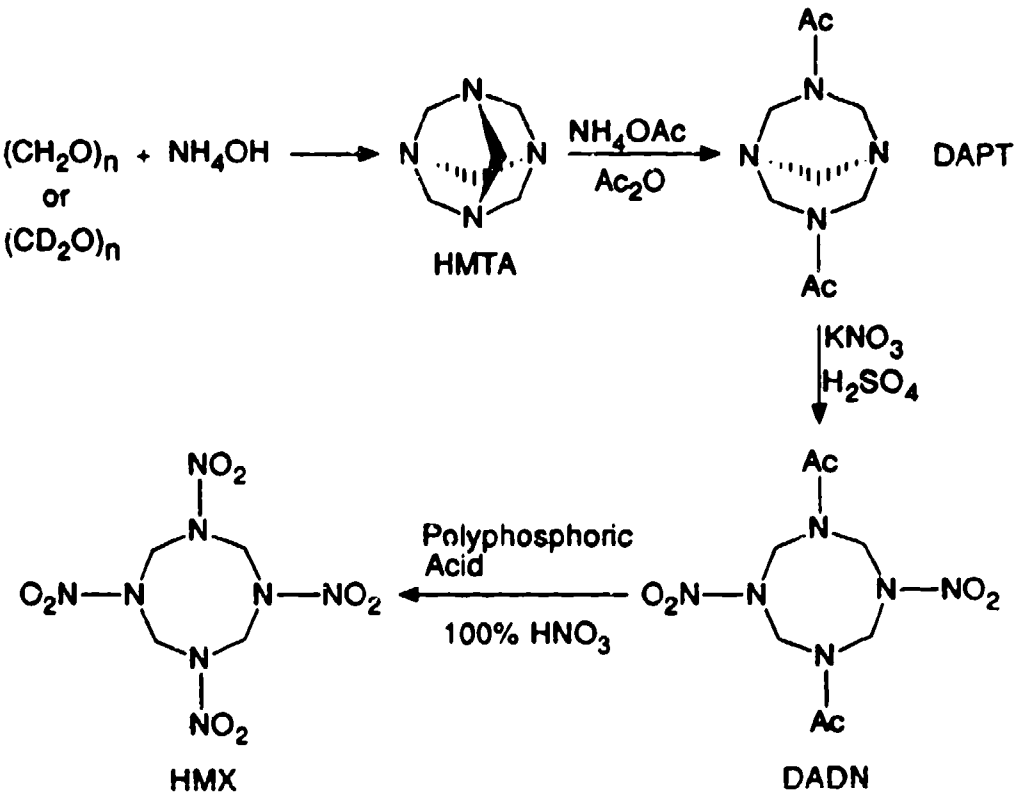

FIGURE 8. HMX Synthesis.

Hexamethylenetetramine (HMTA).[16,58,60] To 11.58 g (0.386 mol) of paraformaldehyde slurried in 20 mL of distilled water was added 20 mL of concentrated NH_4OH (28–30% NH_3) over a 20–30 minute period while

maintaining the reaction temperature at 25–35 °C. After the addition of the ammonium hydroxide was complete, the reaction solution was heated in an oil bath at 35–40 °C for 24 hours. Water was removed from the reaction mixture under vacuum until a wet solid remained. The moist solid was dissolved in 200 mL of methylene chloride giving two layers. The CH_2Cl_2 layer was removed and the remaining aqueous layer was extracted with 4X50 mL CH_2Cl_2. The combined methylene chloride extracts were dried over 1 g of $MgSO_4$. The aqueous layer was then added to 100 mL of CH_2Cl_2 and dried over 5 g of $MgSO_4$. The methylene chloride solutions were filtered and the $MgSO_4$ washed several times with CH_2Cl_2. Following filtration, the methylene chloride was removed under vacuum, leaving a clean white powder.

Yield 8.67 g (96%), m.p. 255-260 °C (decomposes), ^1H NMR ($CDCl_3$) δ 4.66 (-CH_2-).

Hexamethylenetetramine-d_{12} (HMTA-d_{12}).[60] The HMTA-d_{12} was synthesized using 15.00 g (0.468 mol) of paraformaldehyde-d_2 in the same manner as the HMTA described above.

Yield 11.33 g (95%), m.p. 258-265 °C (decomposes).

1,5-diacetyl-octahydro-3,7-*endo*-methylene-1,3,5,7-tetrazocine (DAPT).[60,61] To 8.65 g (0.06 mol) of HMTA was added 3.51 g (0.05 mol) of NH_4OAc and 1.6 mL of distilled water. An overhead mechanical stirrer was used to mix the wet solid while 16.6 g of (0.016 mol) of acetic anhydride was added over a one hour period. During the addition of the acetic anhydride the reaction temperature was maintained at 5–10 °C. After completion of the acetic anhydride addition, the stirred solution was heated at 35–40 °C for 22 hours. The reaction yielded approximately 25 mL of a clear viscous liquid. Half of this

liquid was used for the synthesis of DADN without isolation of the DAPT.

1,5-diacetyl-octahydro-3,7-*endo*-methylene-1,3,5,7-tetrazocine-d_{10} (DAPT-d_{10}). The DAPT-d_{10} was synthesized using 9.39 g (0.06 mol) of HMTA-d_{12}. The remainder of the synthesis was identical to the synthesis of DAPT described above.

1,5-diacetyl-octahydro-3,7-dinitro-1,3,5,7-tetrazocine (DADN).[16,60,61] A total of 16.98 g (0.168 mol) of KNO_3 was slowly added to 55 mL of concentrated H_2SO_4 while maintaining 25–30 °C. Half the DAPT solution from above (~12.5 mL) was then added to the acid solution at a rate such that the reaction temperature remained at 25–30 °C. During and after the addition of the DAPT solution, vigorous stirring from an overhead mechanical stirrer was required to effect complete mixing of the two-phase system. When the addition of DAPT was complete, the solution was stirred for an additional hour at 25–35 °C. The reaction was quenched into 500 g of ice water and then placed into a refrigerator where the DADN product crystallized overnight. The product was suction filtered, washed with water, and air dried.

Overall yield for DAPT and DADN 7.44 g (83%), m.p. 264-265 °C. ^{1}H NMR (DMSO-d_6) of DADN gave δ 2.22 (-CH_3), δ 5.51 (-CH_2-).

1,5-diacetyl-octahydro-3,7-dinitro-1,3,5,7-tetrazocine-d_8 (DADN-d_8).[60] The DADN-d_8 was synthesized using half of the DAPT-d_{10} solution (~12.5 mL) in the same manner as the synthesis of DADN described above.

Overall yield for DAPT-d_{10} and DADN-d_8 7.46 g (80%), m.p. 264–265 °C, ^{1}H NMR confirmed 99% isotopic purity calculated from the acetyl methyl protons.

Octahydro-1,3,5,7-tetranitro-1,3,5,7-tetrazocine (HMX).[16,60,61] In the

synthesis of HMX the configuration of the reaction apparatus can significantly affect product yield. We chose to use a relatively large reaction flask (500-mL three-neck round-bottom) to allow for a greater volume above the reaction mixture. A gas bubbler filled with high vacuum silicone oil was used to limit the venting of NO_2 and N_2O_5 produced during the reaction and prevent the inflow of atmospheric moisture. The conceptual basis of the apparatus configuration was to maintain a positive pressure of NO_2 and N_2O_5, the actual nitrating agent, in the reaction flask. As with the DADN synthesis, vigorous stirring was employed by means of an overhead mechanical stirrer. A small amount of anhydrous nitric acid was used to lubricate the shaft of the mechanical stirrer.

To 78 g of polyphosphoric acid was added 35.3 g of anhydrous HNO_3. These acids were mixed until they became a homogeneous viscous liquid. A total of 6.40 g (0.022 mol) of DADN was added rapidly to the acid mixture. The reaction was then heated at 60 °C with stirring. As the reaction progressed, the atmosphere above the solution gradually changed from a light red initially to a dark red-brown by the end of the reaction. After one hour the reaction was allowed to cool to 40 °C and then quenched by pouring on 300 g of finely crushed ice. The resulting mixture was then filtered, washed thoroughly with water, and air dried. The product consisted of fine white needle-like crystals (Fig. 9), which are indicative of the α form of HMX. The β-polymorph of HMX was obtained by dissolving the α-HMX in acetone and then gradually removing the solvent with vacuum. The conversion to β-HMX was confirmed using optical microscopy (Fig. 10).

Yield β-HMX 4.98 g (76%), m.p. 279–280 °C, ^{1}H NMR (DMSO-d_6) δ 6.02 (-CH_2-). The DADN methylene peak at δ 5.52 was absent from the NMR spectrum, indicating that nitration was greater than 98% complete.

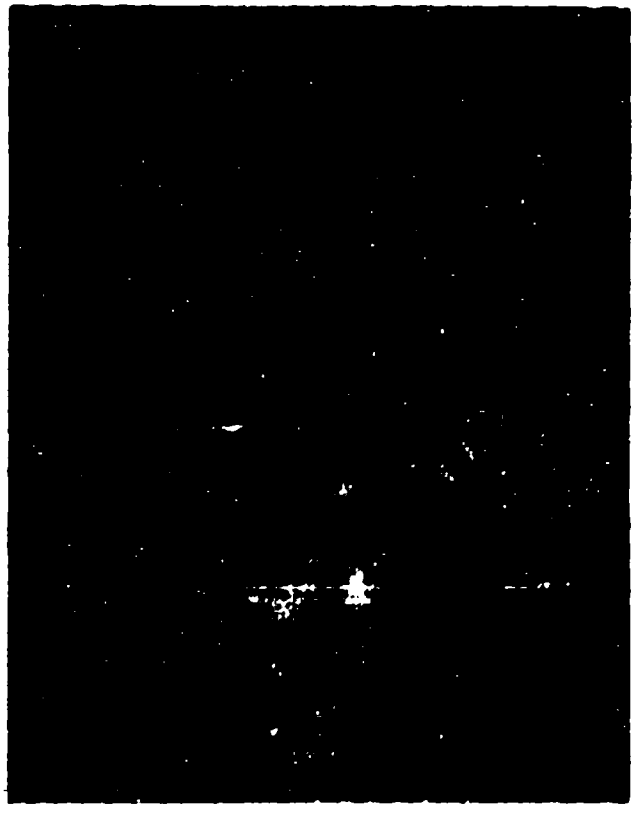

FIGURE 9. α-HMX.

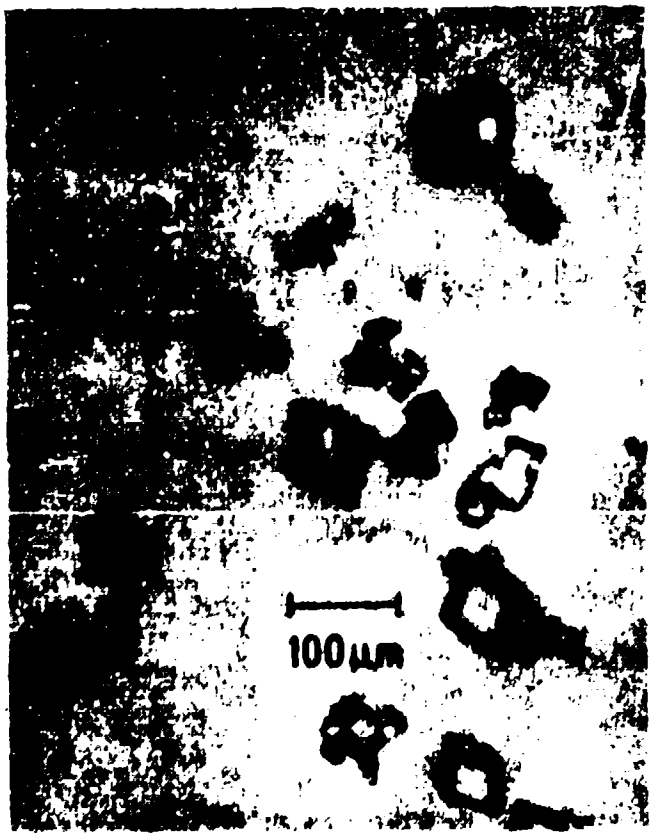

FIGURE 10. β-HMX.

Octahydro-1,3,5,7-tetranitro-1,3,5,7-tetrazocine-d_8 (HMX-d_8).[16,60,61] The HMX-d_8 was synthesized using 6.56 g of DADN-d_6 in an identical manner to HMX described above. Yield β-HMX-d_8 5.24 g (80%), m.p. 279–280 °C, ^{1}H NMR showed small peaks at δ 5.52 and δ 6.02 corresponding to approximately 0.5% DADN-d_8 and the equivalent of 0.5% HMX-h_8 respectively.

Synthesis of RDX

The synthesis of RDX begins with the preparation of HMTA as does the synthesis of HMX. However, in contrast to HMX, the preparation of RDX involves the conversion of HMTA to 1,3,5-triacetyl-hexahydro-1,3,5-triazine (TRAT). Furthermore, the final nitration step where TRAT is converted to RDX requires a slightly stronger nitration reagent (HNO_3/P_2O_5) than the HNO_3/ polyphosphoric acid used in the HMX synthesis to give RDX. The three step synthesis of RDX is diagramed in Figure 11 and described in detail in the text below.

1,3,5-triacetyl-hexahydro-1,3,5-triazine (TRAT).[62,64] Hexamethylene-tetramine, 8.3 g (0.059 mol), was added to 34.3 g (0.34 mol) of acetic anhydride at room temperature with stirring. The resulting solution was heated at 98 °C for two hours. This being complete, the reaction mixture was cooled to 5 °C, 20 mL of distilled water was added, and the resulting mixture stirred for 30 minutes. The solution was then reduced to a viscous yellow liquid under vacuum. Distilled water (20 mL) was added, the mixture was cooled, and seed crystals were introduced to induce precipitation. The solid product was then filtered and dried *in vacuo* over NaOH pellets.

Yield 8.65 g (64%), m.p. 95–96 °C, ^{1}H NMR (DMSO-d_6) δ 2.1 (-CH_3), δ 5.2 (-CH_2-).

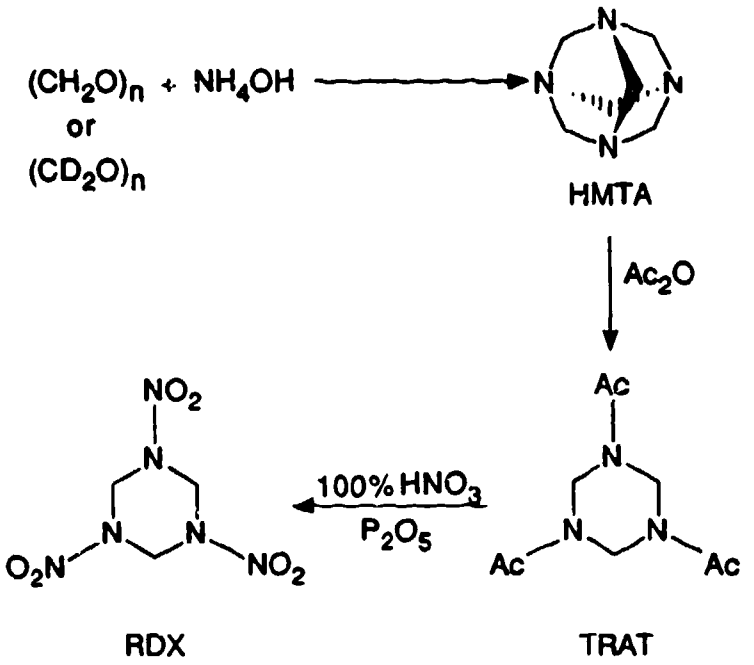

FIGURE 11. RDX Synthesis.

1,3,5-triacetyl-hexahydro-1,3,5-triazine-d_6 (TRAT-d_6).[64] The TRAT-d_6 was synthesized using 7.00 g (0.046 mol) of HMTA-d_{12} and 28.7 g (0.28 mol) of acetic anhydride in the same manner described for the TRAT synthesis above.

Yield 7.60 g (75%), m.p. 95–96 °C, ^{1}H NMR of TRAT-d_6 showed greater than 98% deuterium substitution on the ring methylene groups calculated from the acetyl methyl protons.

Hexahydro-1,3,5-trinitro-s-triazine (RDX).[59,62,64] As with the final nitration step in the synthesis of HMX, the composition of the atmosphere above the nitrating solution significantly affects product yield. An apparatus identical to the one used for the nitration of DADN was employed for the nitration of TRAT.

To 5.4 g (0.378 mol) of phosphorus pentoxide (weighed out under nitrogen) in a three-neck 500-mL round-bottom flask was added dropwise 108

mL of anhydrous nitric acid. The addition of the HNO_3 caused an exotherm to 41 °C. An overhead mechanical stirrer was utilized to ensure complete mixing of the HNO_3 and P_2O_5. The mixture was cooled to 36 °C and 5.4 g (0.026 mol) of TRAT was added rapidly. The reaction flask was placed in an oil bath and heated at 65 °C for 15 minutes. As the temperature increased, the atmosphere above the reaction mixture changed from a light yellow to a dark red-brown. The reaction mixture was allowed to cool to room temperature and then poured on ice. After the ice melted the white precipitate was filtered, washed with water, and allowed to air dry.

Yield 4.00 g (71%), m.p. 202-203 °C, ^{1}H NMR (DMSO-d_6) δ 6.1 (-CH_2-).

Hexahydro-1,3,5-trinitro-s-triazine-d_6 (RDX-d_6).[64] RDX-d_6 was synthesized, using 5.55 g (0.0253 mol) of TRAT-d_6, following the procedure described for the synthesis of RDX.

Yield 4.00 g (69%), m.p. 203–204 °C, ^{1}H NMR spectrum showed greater than 98% isotopic integrity.

HMX and RDX Particle Size

The 90%, 50%, and 10% particle diameters and the calculated specific surface area for each of the four synthesized nitramines are listed in Table IV.[65] The particle diameter data were obtained using a Malvern 3600E Particle Size Analyzer. The Malvern analyzer collects data by using a light scattering technique to determine the number of particles in each of a large number of diameter bands. Using these data the diameters listed in Table IV were calculated. An example of how the data in Table IV are interpreted is as follows: the particle size listed for the 90% diameter is simply the diameter below which 90% of the sample particle diameters fall. The Malvern determines

the surface area of each band using the median diameter of the band and assuming that all particles are perfect spheres. The specific surface area for a sample is simply the sum of the surface areas for all the diameter bands. Because many particle samples do not possess a normal distribution of sizes, it is perfectly conceivable that two samples with different particle distributions can have the same specific surface area.

TABLE IV

Particle Diameters (microns, μm) and
Calculated Specific Surface Area (m^2/cm^3)

Compound	90%	50%	10%	Specific Surface Area
HMX	47.4	21.9	6.2	0.13
HMX-d_8	60.3	35.7	8.6	0.10
RDX	61.2	36.7	11.8	0.10
RDX-d_6	53.7	22.8	8.3	0.11

DSC EXPERIMENTS

The $\beta \rightarrow \delta$ phase transition of HMX and HMX-d_8 was investigated using a Perkin-Elmer Model DSC-4 Differential Scanning Calorimeter. Experiments consisted of placing the sample (either 5.0 or 10.0 ± 0.2 mg) in a sealed aluminum sample pan, Perkin-Elmer Part No. 219-0041, and then performing a normal DSC experiment scanning from 150 to 200 °C at 5 °C/min. Following the completion of the experiment, peak analysis was performed on the phase transition endotherm to determine the onset temperature, the peak temperature, and the heat of transition.

COMMERCIALLY OBTAINED CHEMICALS

The ingredients used in the model propellant formulations were standard propellant grade unless otherwise noted and were obtained from the following manufacturers: dibutyltin diacetate (DBTDA), reagent grade, Alfa Products; hydroxyl-terminated polybutadiene (HTPB, trade name R-45M) Lot #803445, ARCO; isophorone diisocyanate (IPDI) Lot #6932-0008, Chemischewerke Hüls AG; poly(diethyleneglycol adipate) hydroxyl-terminated (trade name R-18) Lot #D-018 4-002, Mobay; trimethylolethane trinitrate (TMETN) Lot #6H-10M, Trojan; triphenyl bismuthine (TPB), reagent grade, Aldrich.

For experiments not requiring isotopically labelled nitramines, propellant grade HMX and RDX were used. The HMX, Lot #78L675-014 and weight median diameter of 26 μm, and the RDX, Lot #77H150-058 and weight median diameter of 35 μm, were obtained from Aerojet Corporation.

PRESSED PELLET PREPARATION

The bottom halves of No. 3 gelatin capsules (Eli Lilly Co.) were used to contain the pressed nitramine powder and to act as an inhibitor to ensure the uniform horizontal burning of the pellets. The pellets were prepared by first placing the gelatin capsule into the pellet die (Figs. 12 and 13) then filling the capsule with the appropriate nitramine powder. The powder was then lightly compressed to allow for the addition of more nitramine; more powder was added and then compacted. This compacting procedure was repeated several times until the level of the pressed powder was a few millimeters above the top lip of the capsule. A hydraulic press (Model-C, Fred S. Carver Inc.) and a punch (dia. 0.208 in), which fit snugly inside the gelatin capsule (I.D. 0.211 in), was used to compress the powder to a pressure of 50 psi on a 1-7/8 inch ram (Fig. 12). The punch was then withdrawn and more powder added to a level above

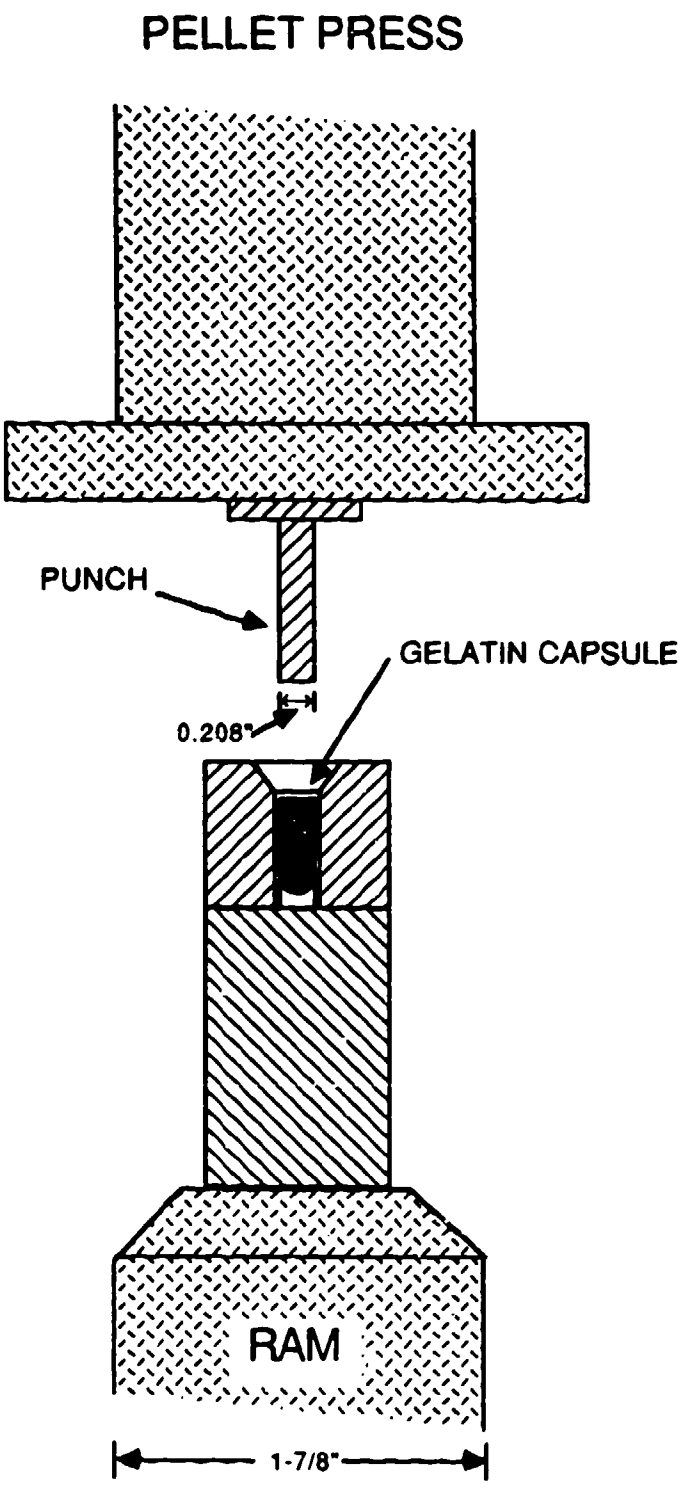

FIGURE 12. Pellet Pressing Apparatus.

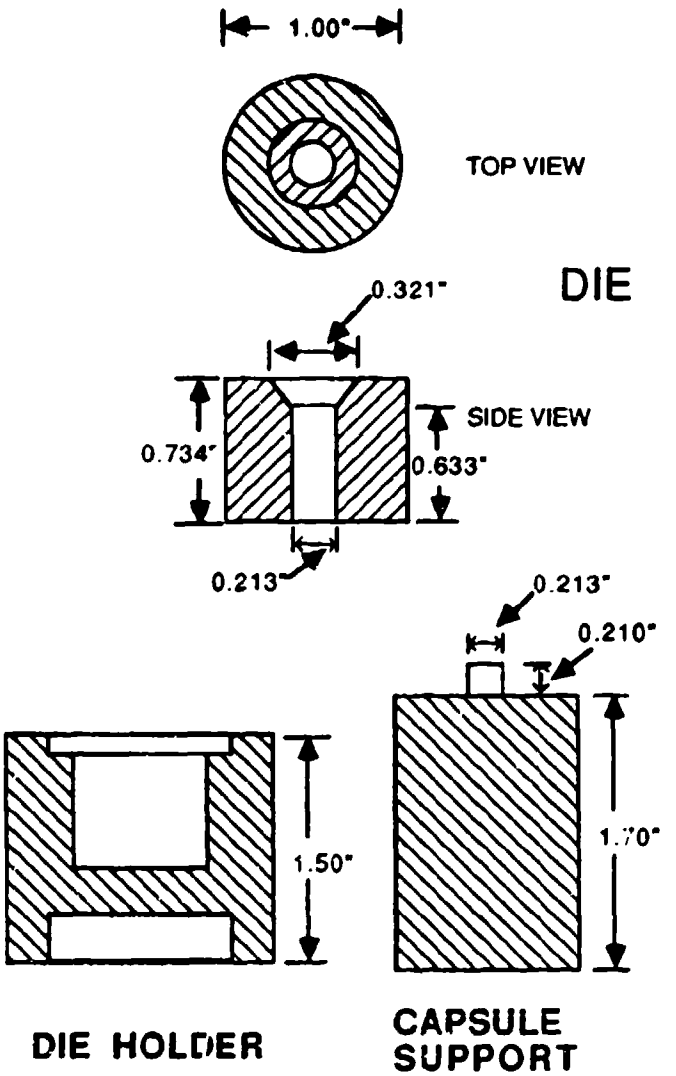

FIGURE 13. Pellet Die, Holder, and Capsule Support.

the capsule lip. The powder was then pressed to its final pressure of 100 psi on the 1-7/8 inch ram. This final pressure equates to a pressure on the 0.211-inch diameter pellet of 7,900 psi. The powders were pressed to this pressure in order to give pellet densities approximately the same as the densities of the formulated propellants.

The pellet was removed by placing the die with capsule onto the die holder (Fig. 13) and pressing the capsule out the bottom of the die with the punch. A razor blade was used to shave off the excess powder down to the top lip of the gelatin casing. The densities of the RDX, RDX-d_6, HMX, HMX-d_8 pellets are listed in Table VIII along with the densities of the propellant pellets. After pressing, the pellets were approximately 13 mm by 5.4 mm.

MODEL PROPELLANT PREPARATION

Propellant Formulations

The nitramine propellant formulations used in this study, designated CW5, PB, and RRHR-18, are listed in Tables V, VI, VII respectively. The CW5 formulation (Table V) was chosen because of its simplicity and because it contained both an energetic plasticizer and a high oxygen content polymer.[66] The CW5 formulation is a relatively energetic nitramine propellant which burns very uniformly owing to an almost equal balance between fuel and oxidizer components.

The PB propellant formulation was also chosen for its simplicity. In addition, it has been used previously in studies involving both combustion modeling[67] and propellant burning properties.[68] Thus, a large amount of information exists dealing with the PB propellant burning characteristics. The PB propellant is much less energetic than the CW5 propellant. It has a fuel rich

formulation which burns in a very heterogeneous manner giving off a great deal of carbonaceous residue. The CW5 and PB propellants represent the opposite extremes as far as energetics and burning properties, and therefore they should provide a relevant test of isotope effects in cured nitramine propellants.

TABLE V

CW5 Propellant Formulation

Compound	Percent
Nitramine	73.20
R-18 (polymer) 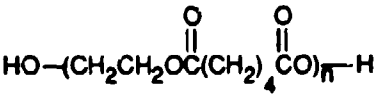	8.51
TMETN (plasticizer) 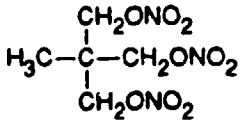	16.89
IPDI (curative) 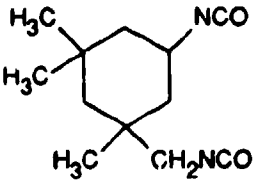	1.39
DBTDA (cure catalyst) $Bu_2Sn(OAc)_2$	0.01

The RRHR-18 propellant formulation was not used in any isotope effect experiments. It was designed to provide an additional propellant to study the effects of combustion pressure and propellant formulation on flame structure and burning surface characteristics.

TABLE VI

PB Propellant Formulation

Compound	Percent
Nitramine	80.00
R-45M (polymer)	18.52
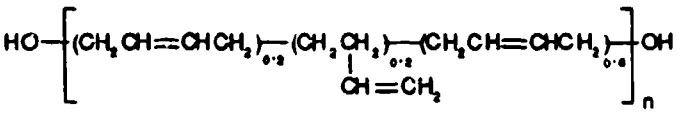	
IPDI (curative)	1.46
TPB (cure catalyst) $(C_6H_5)_3Bi$	0.02

TABLE VII

RRHR-18 Propellant Formulation

Compound	Percent
Nitramine	80.00
R-18 (polymer)	17.17
IPDI (curative)	2.81
DBTDA (cure catalyst)	0.02

Propellant Binders

In our experiments two different types of binders were used. The binder of the CW5 and RRHR-18 formulations employed a polyester polymer R-18 which was 37% by weight oxygen and had a number average molecular weight of 1400. The CW5 formulation also employed a nitrate ester plasticizer

TMETN, which increased the energy of the binder in addition to increasing binder elasticity. The PB formulation used a polybutadiene polymer R-45M, which was 3.6% by weight oxygen with a number average molecular weight of 2800. Because the PB and RRHR-18 formulations did not contain a plasticizer, their binder was much harder than that in the CW5 formulation.

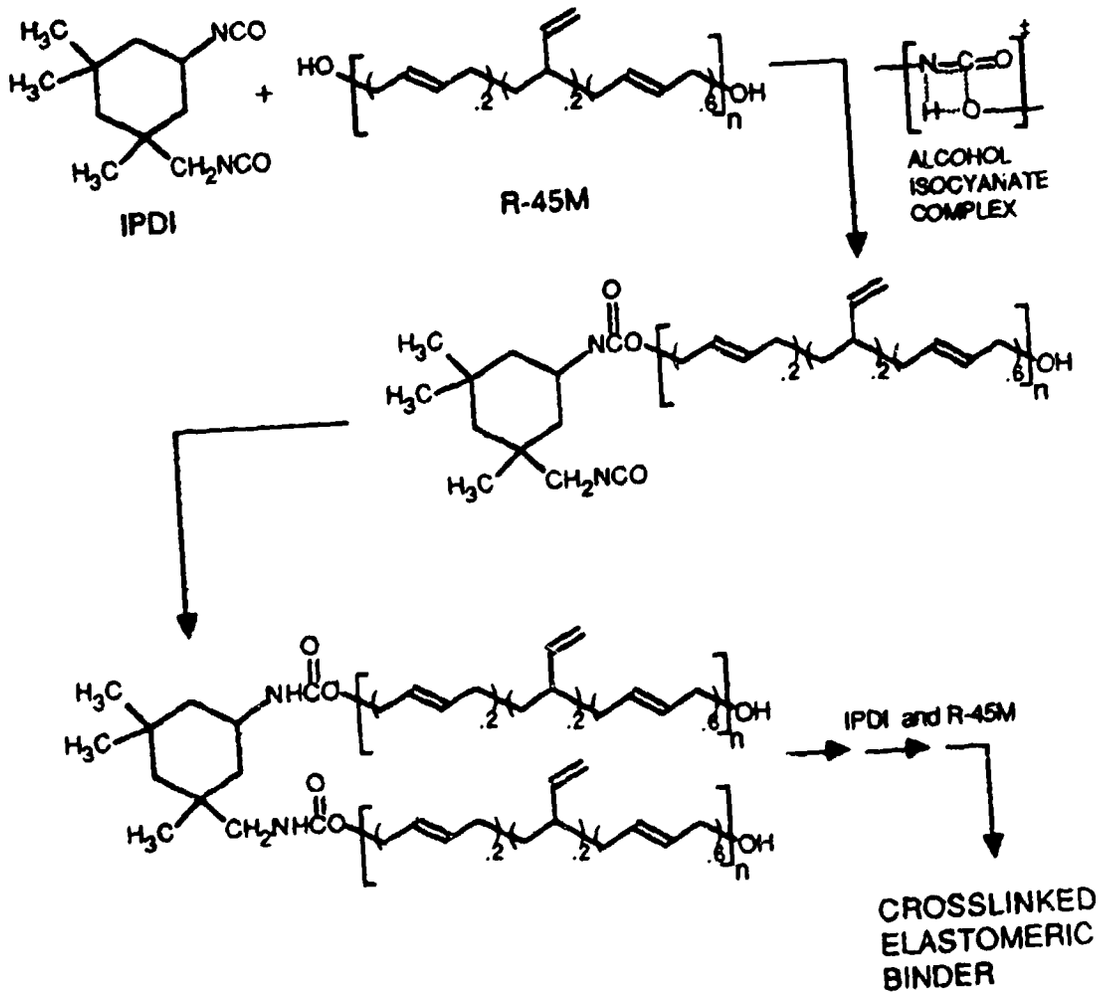

FIGURE 14. Urethane Cure of the R-45M Polymer.

Both polymers were crosslinked using a so called "urethane cure." This involves the condensation reaction of the isocyanate curative with the hydroxyl end group on the polymer to form a urethane linkage (Fig. 14).[69] The cure catalyst appears to facilitate the curing process by stabilizing the alcohol-isocyanate complex thus enhancing the rate of formation of the urethane linkages.[70]

The elastomeric binder consists of a three dimensional matrix of polymer units linked together by the isocyanate curative. The amount of curative used dictates the amount of crosslinking in the binder and thus significantly affects the bulk properties of the binder. In the case of the CW5, RRHR-18, and PB formulations, a one-to-one mole ratio of polymer to curative was used.

CAUTION: Care must be taken while mixing and handling the HMX and RDX propellants due to their explosive nature. Solid Teflon utensils and beakers were used at all times in the propellant preparation to preclude accidental spark ignition.

Propellant Mixing

The propellants were prepared on a 2.5-g scale in a 50-mL Teflon beaker. Initially, the polymer, curative, and, if necessary, plasticizer w. e mixed into a viscous homogeneous liquid. The nitramine, which had been dried at 60 °C for 12 h, was then mixed in until a smooth, pasty consistency was achieved. Finally, the cure catalyst was added and the completed propellant carefully packed into the bottom halves of five No. 3 gelatin capsules. Great care was taken to avoid leaving any trapped air in the propellant. The propellant-filled capsules were then cured at 40 °C in a pressure bomb (Parr Model 1108

Oxygen Bomb) pressurized to 50 atm with nitrogen. The CW5 and RRHR-18 propellants were fully cured after 12 h at 40 °C. However, the PB propellants required from 24 to 36 h at 40 °C to fully cure. The density of the propellants are listed in Table VIII. The cured CW5, RRHR-18, and PB propellant pellets were approximately 13.5 mm by 5.4 mm.

TABLE VIII

Pellet Densities for the Pressed Powders and the Formulated Propellants

Pellet Type	Density (g/cm^3)[a]
HMX / HMX-d_8	1.525 ± 0.015
RDX / RDX-d_6	1.400 ± 0.010
HMX / HMX-d_8 CW5	1.616 ± 0.015
RDX / RDX-d_6 CW5	1.480 ± 0.030
HMX / HMX-d_8 PB	1.507 ± 0.016
RDX / RDX-d_6 PB	1.395 ± 0.025
HMX RRHR-18	1.554 ± 0.0[illegible]
RDX RRHR-18	1.423 ± 0.0[illegible]0

[a] The reported error is at the 95% confidence level.

PVC Coated Propellants

The gelatin capsules frequently cracked due to dehydration when propellant curing required more than 24 h. Because the propellant burning surface propagated down these cracks, making accurate burn rate determination almost impossible, the damaged gelatin capsules did not function

effectively as burning inhibitors. Therefore, several experiments were performed using a polyvinyl chloride (PVC) coating as the burning inhibitor. This was accomplished by first preparing the propellant in the gelatin capsules as described above. The fully cured encapsulated propellants were then placed in a dilute aqueous acetic acid solution to dissolve away the gelatin. The propellant pellets were then thoroughly washed with distilled water and air dried. The pellets were dipped into a dilute solution of PVC in methylene chloride and air dried. Finally, a razor blade was used to shave off a small disk of propellant from the top of the pellet to give an uncoated surface for burning.

WINDOW BOMB COMBUSTION PROCEDURE

Burn rate experiments were performed in a reinforced concrete test cell at the Air Force Astronautics Laboratory, Propellant Experimental Area 1-30. All experiments were monitored remotely from a control room adjacent to the test cell.

Window Bomb

The window bomb (AFRPL Window Bomb drawing #X7616176) used for all combustion experiments is shown in Figure 15. Samples in the window bomb were illuminated using a xenon spot light (Color Arc 2000). Experiments were recorded using a high speed video system (Ektapro 1000, Kodak-Spin Physics). Data was collected at a rate of 1000 frames per second with timing data recorded on each video frame.

Burn Rate Experiments

A typical burn rate experiment began by first placing a ruler on the base of the window bomb in the same location as occupied by the pellet (Fig. 16a). The base was then screwed on to the bomb and approximately one hundred

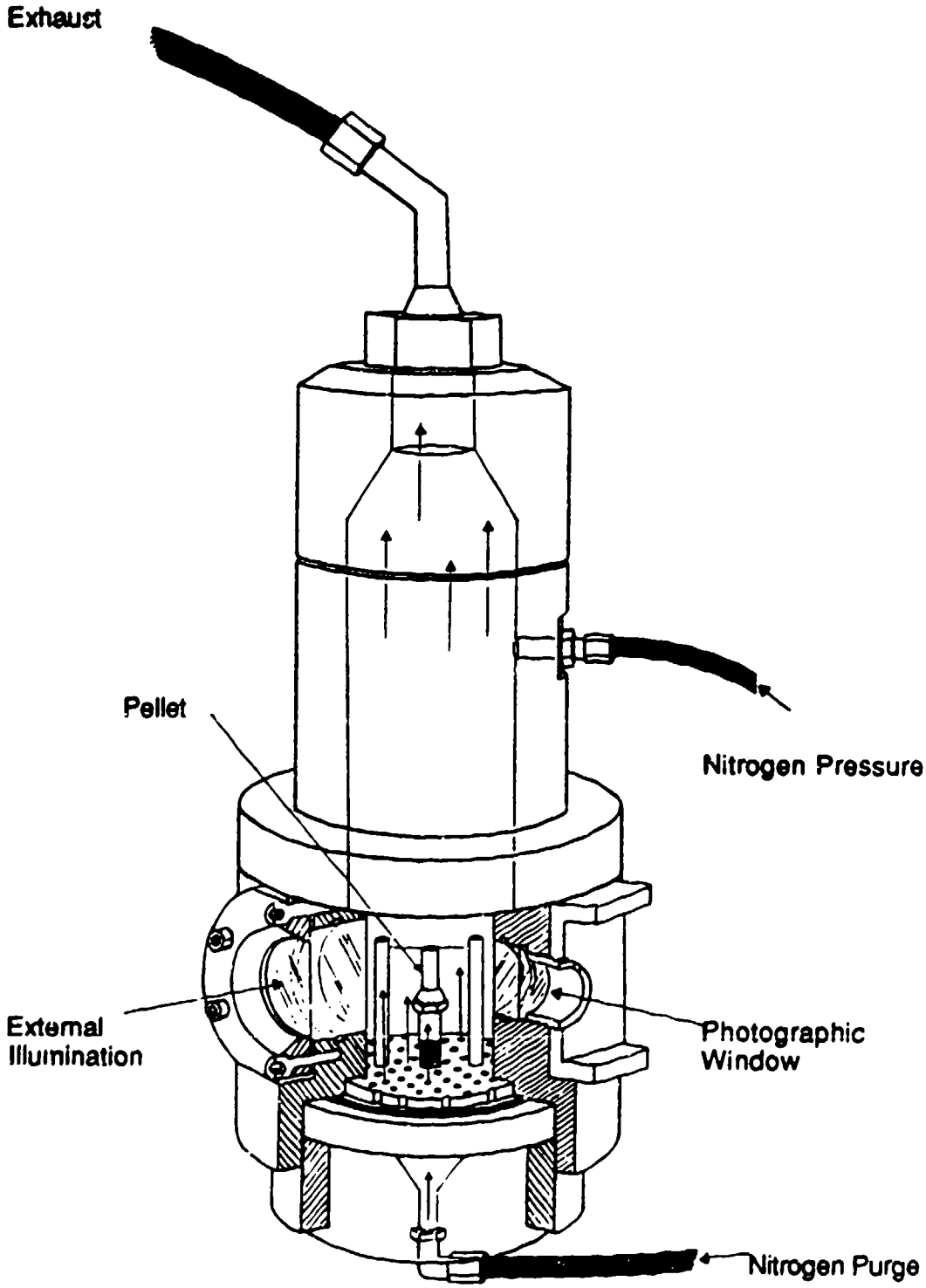

FIGURE 15. High Pressure Window Bomb.

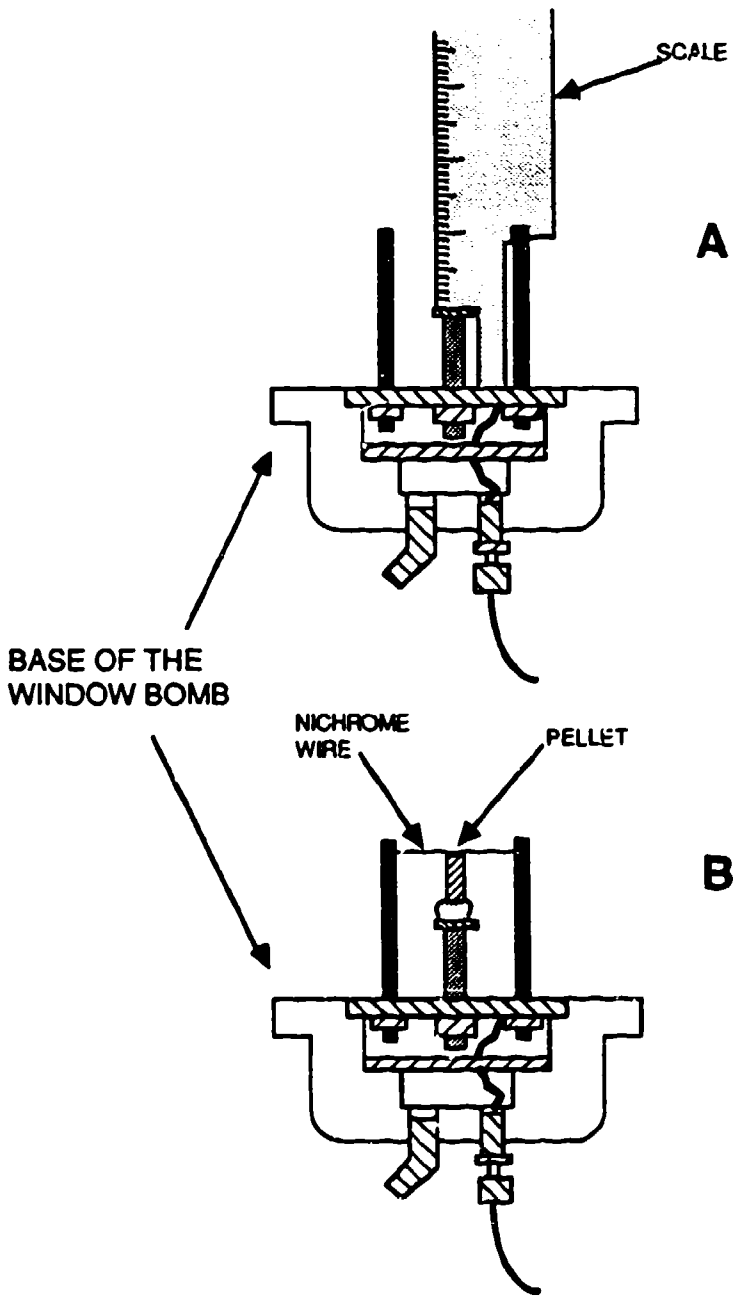

FIGURE 16. Placement of Pellet and Scale.

frames of the scale were taken using the high speed video system. These data were later used to determine burn rates. The scale was then removed and replaced with a pellet placed atop a small piece of putty (Fig. 16b). The pellet, with a Nichrome wire stretched across the top, and the base were then attached to the bomb. Normally the window bomb was pressurized to 1000 psi with nitrogen prior to the experiment. The pressure inside the window bomb was regulated to ± 10 psi during the experiment. A constant 15 psid (a 15 psi differential between inlet and exit pressures) nitrogen purge during the experiment maintained a clear photographic path to the pellet by removing combustion products and dissipating convective heat currents. The pellet was ignited by the Nichrome wire and the burning recorded using the high speed video system.

Burn rates were determined in the following manner. A single video frame of the ruler inside the window bomb was displayed on a video monitor. A clear mylar sheet containing a grid which exactly matched the ruler markings displayed on the monitor was taped to the screen. The video of the pellet burn was then advanced until all the effects of ignition had dissipated. This was normally after about the top 20% of the pellet had burned. At this point the time given on the video frame and the distance on the grid were recorded. The video was then advanced until the pellet burn reached the point where the curvature of the pellet bottom began. At this location the time and distance were again recorded. The pellet burn rate was calculated simply by taking the distance burned over the change in time.

Extinguishing Burning Propellants

In order to observe the composition and structure of the propellant burning surface, several burning pellets were extinguished through rapid

decompression of the combustion chamber. To begin, the procedure followed exactly that used for normal pellet burns. However, once the pellet was ignited, the combustion chamber was vented to the outside atmosphere, causing rapid decompression and extinguishing the burn. Decompression from 1000 psi to ambient pressure required approximately one second.

Electron micrographs of the propellant burning surfaces were obtained using an ISI CL-6 scanning electron microscope (SEM). Samples were coated with a gold film prior to SEM examination using a Hummer X sputter coater to facilitate the efficient conduction of electrons away from the propellant surface.

RESULTS AND DISCUSSION

The linear burn rate of nitramines and nitramine propellants depends on both kinetic and physical parameters.[3,68] In our experiments, factors such as pressure, temperature, the shape and size of the burning surface, etc. are essentially the same for two samples differing only by isotopic substitution. Thus any burn rate differences should be due to the effect of isotopic substitution on the rate limiting process in the combustion mechanism. Because it is virtually impossible to obtain kinetic rate constants from combustion experiments, burn rates must be used to obtain isotope effect values. Thus, to make any conclusions about the rate limiting process from KDIE values one must understand the relationship between burn rate and the kinetic rate constant of the combustion reaction.

Nitramine and nitramine propellant combustion begins with condensed phase decomposition reactions at the burning surface and proceeds through to gas phase oxidation reactions in the luminous flame.[3,16,71] Reaction temperatures for combustion range from approximately 673 K at the burning surface to in excess of 1800 K in the luminous flame.[68] A fundamental principle of reaction kinetics is that reaction rates increase with increasing temperature.[73] In addition, it can be shown that reaction rates tend to increase when going from a non-mobile condensed phase to the gas phase.[74] Thus, it would seem, *a priori*, that the slowest reactions in the combustion mechanism occur in the

condensed phase. The numerous mechanistic models proposed for HMX and RDX condensed-phase decomposition suggest a limited number of reactions occurring in the condensed phase due to the early production of gas-phase intermediates.[6,8,11,19,75] Recent theoretical studies indicate that after the early bond breaking steps of HMX and RDX decomposition, the further breakup of the nitramine becomes relatively facile.[76] From this, one can reasonably conclude that it is likely that the slowest step in the nitramine combustion mechanism occurs early in the condensed-phase nitramine decomposition.

Depending on the initial conditions, the decomposition of HMX and RDX follow either a first order (eq. 24)[17,20,77,78] or an autocatalytic rate law (eq. 25).[19]

$$\frac{d\alpha}{dt} = k(1-\alpha) \tag{24}$$

$$\frac{d\alpha}{dt} = k\alpha(1-\alpha) \tag{25}$$

The extent of reaction is represented by α, t is time, and k is the kinetic rate constant for the reaction. It can be shown that

$$\frac{d\alpha}{dt} = rC \tag{26}$$

where r is the linear burn rate and C is a shape factor which depends on the dimensions of the burning surface.[79] Assuming the same process that controls the rate of decomposition controls the rate of combustion, then with respect to the equations above (eq. 24, 25, and 26), the linear burn rate should be proportional to the kinetic rate constant such that KDIE values can be obtained from burn rates by using the following equation.

$$\frac{r_H}{r_D} = \frac{k_H}{k_D} \tag{27}$$

We have assumed equation 24 to be valid, and have used it to calculate all KDIEs presented in this thesis.

The rate constant k for the combustion reaction is dependent on the rate constant of the slowest step and to a lesser extent on the steps preceding the slow step.[73] Since the rate controlling process for nitramine combustion appears to occur early in the decomposition, the value of k should reflect primarily the rate constant of the slow step. Thus, the KDIE values obtained from burn rates should be reasonably representative of the effect of deuterium substitution on the rate controlling process

Results from the computational modeling of nitramine propellant burn rates suggest that k is proportional to r^2 instead of r.[67,80-85] However, these combustion modeling studies are generally empirical in nature and only loosely based on kinetic data. Therefore, it is difficult to attach any significance to the implications of the modeling results. Even if k were proportional to r^2, this would simply mean that the true KDIE values for the nitramine and nitramine propellant combustion reaction rate constants would be some what larger than the values shown in this thesis (in particular, the square of the KDIEs based on r). In the end this would not significantly affect the interpretations we have made.

BURN RATE EXPERIMENTS

It was the intent of the following experiments to measure the relative burn rate differences between samples containing either the protiated or deuteriated nitramine. Additionally, it was our purpose to compare the KDIEs of the pure nitramines with the KDIEs of the corresponding propellant mixtures. Toward this end, every effort was made to preclude differences in burn rate due to

synthesis, sample history, propellant mixing, pellet preparation, and pellet density.

Pressed Pellet Results

As a baseline for future comparison to model nitramine propellants we duplicated the previous[16,17] combustion studies on HMX, HMX-d_8, RDX, and RDX-d_6 pressed pellets, acquiring the burn rate data listed in Table IX. The burn rates of commercial grade HMX and RDX pressed pellets were also measured giving values of 0.535 ± 0.057 in/s and 0.551 ± 0.020 in/s, respectively. These burn rates are in the same range as the values listed for the synthesized HMX and RDX indicating the results given in Table IX are reasonable.

TABLE IX

Burn Rate Results for HMX, HMX-d_8, RDX, and RDX-d_6 Pressed Pellets at 1000 psi.[a]

HMX (r_H)[b]	HMX-d_8 (r_D)[b]	RDX (r_H)[b]	RDX-d_6 (r_D)[b]
0.503	0.394	0.600	0.449
0.505	0.386	0.587	0.456
0.531	0.395	0.609	0.457
0.503	0.397	0.578	0.452
$\bar{r}_H = 0.510 \pm 0.022$	$\bar{r}_D = 0.393 \pm 0.008$	$\bar{r}_H = 0.594 \pm 0.022$	$\bar{r}_D = 0.454 \pm 0.006$

$$KDIE = \left(\frac{\bar{r}_H}{\bar{r}_D}\right) = 1.30 \pm 0.04 \qquad KDIE = \left(\frac{\bar{r}_H}{\bar{r}_D}\right) = 1.31 \pm 0.03$$

[a] Reported error is at the 95% confidence level. [b] Values reported in in/s.

The KDIE of 1.40 ± 0.11 for HMX combustion at varying pressures (500–1500 psi) reported previously by Shackelford et al.[16] is consistent with our 95% confidence interval of 1.30 ± 0.04 for the mean isotope effect for HMX. The previous report of 1.46 ± 0.23 for RDX[17] under conditions identical to ours (1000 psi) is also consistent with our estimate of 1.31 ± 0.03 for pure RDX.

Using the evaluation criteria developed in the previous chapter, the estimate for the isotope effect arising from a C-H bond rupture in HMX or RDX is 1.41 (see page 37). The estimated isotope effect for a C-N bond rupture is 1.19 (see page 37). These estimates were made from data collected at temperatures around 500 K, whereas the temperature of the burning surface during combustion is approximately 673 K. If one used equation 16 and assumed that the isotope effects were due strictly to zero point energy differences (i.e., $[\Delta E_a]_D^H$), then a temperature extrapolation can be performed on the above estimates giving KDIE values of 1.29 for a C-H bond rupture and 1.14 for a C-N bond rupture at 673 K.

The rate limiting process for the decomposition of HMX and RDX under most circumstances appears to be a C-H bond rupture.[17,19,20] Assuming a consistent rate limiting process for both decomposition and combustion and applying the above KDIE criteria for 673 K, the isotope effect values for both HMX and RDX of 1.30 ± 0.04 and 1.31 ± 0.03, respectively indicate a rate limiting C-H bond rupture in the combustion process. These assignments are in agreement with the previous HMX and RDX combustion studies.[16,17]

Effects of Curing Conditions and Burning Inhibitors

The effects of curing conditions and burning inhibitors on propellant burn rate were investigated in order to test the ruggedness of our CW5 propellant

formulation. The results of these experiments on CW5 propellant formulations containing commercial grade HMX or RDX are listed in Table X.

TABLE X

The Effects of Burning Inhibitor, Curing, and Curing Pressure on CW5 Propellant Burn Rates at 1000 psi.

Formulation	Cure Conditions[a]	Burning Inhibitor	Burn Rate (in/s)[b]
HMX-CW5	1 atm	Gelatin Capsule	0.175 ± 0.006
HMX-CW5	50 atm	Gelatin Capsule	0.166 ± 0.003
HMX-CW5	uncured[c]	Gelatin Capsule	0.158 ± 0.007
HMX-CW5	50 atm	PVC	0.177 ± 0.004
RDX-CW5	1 atm	Gelatin Capsule	0.177 ± 0.003
RDX-CW5	50 atm	Gelatin Capsule	0.178 ± 0.005
RDX-CW5	uncured[c]	Gelatin Capsule	0.174 ± 0.004
RDX-CW5	50 atm	PVC	0.186 ± 0.009

[a] All propellants were maintained at 40 °C until fully cured. [b] Reported error is at the 95% confidence interval. [c] No DBTDA cure catalyst was added to these propellants.

Large scale propellant mixing operations avoid the problem of trapped gases by performing most propellant mixing procedures under a vacuum. However, because it is almost impossible to use normal mixing methods when working on a 2.5 g scale, our initial propellant mixtures were prepared and cured at atmospheric pressure. Not unexpectedly, these propellants contained trapped gases in the form of bubbles in the propellant. When pellets of these propellants were placed inside the window bomb and then pressurized to 1000

psi the sides of the pellets were compressed due to the compression of the bubbles inside the cured propellant. This problem was avoided if the propellant was cured at 50 atm (735 psi). Evidently, the increased curing pressure either forced out or compressed the bubbles in the propellant. As one can see from the data in Table X the effect of the change in curing pressure is very small. There was only a slight decrease in the HMX-CW5 burn rate and no change in the RDX-CW5 burn rate when changing the cure pressure from 1 to 50 atm.

The difference in the burn rate of cured versus uncured HMX-CW5 is relatively small. In the case of the RDX-CW5 propellant the difference is insignificant. These results indicate the relative unimportance of the physical structure of the propellant binder in determining burn rate. Consequently, any differences in crosslinking density, and thus binder physical properties, between identical propellant mixes should not introduce any significant variation in burn rate.

There was a small increase in the burn rate of both HMX and RDX CW5 propellants when the burning inhibitor was switched from a gelatin capsule to PVC. More than likely these differences are due to the different physical characteristics of the inhibitors. The gelatin capsule was better at limiting the propellant burning to the top surface of the pellet. The PVC coating allowed the propellent burning to proceed down the side of the pellet slightly ahead of the advancing top surface; this allowed more burning surface, thus increasing the overall linear burn rate.

Overall one can see from the data in Table X that the variation in parameters had only a minor effect on the CW5 propellant burn rate. Thus one can conclude that any changes in burn rate between normal and deuterium labeled propellants should be due strictly to the effect of deuterium on the rate controlling process.

TABLE XI

Burn Rate Results for HMX and HMX-d_8 CW5 Propellants at 1000 psi.[a]

HMX-CW5 (r_H)[b]		HMX-d_8-CW5 (r_D)[b]
0.173	0.180	0.142
0.174	0.179	0.141
0.178	0.201	0.131
0.159	0.155	0.137
0.162	0.206	0.136
$\bar{r}_H = 0.177 \pm 0.012$		$\bar{r}_D = 0.137 \pm 0.005$

$$KDIE = \left(\frac{\bar{r}_H}{\bar{r}_D}\right) = 1.29 \pm 0.07$$

[a] Reported error is at the 95% confidence level. [b] Values reported in in/s.

KDIE in CW5 Propellant Mixtures

The burn rate results for normal and deuterium labeled HMX and RDX CW5 propellants are listed in Tables XI and XII respectively. Because of the small size of the KDIE for data Set I and the low burn rate of the RDX-CW5 propellant when compared with the burn rate of the commercial grade RDX-CW5 (Table IX), a second set of data was obtained. The burn rates for both the RDX-CW5 and RDX-d_8-CW5 propellants in the second data set were significantly greater than in the first data set. The propellants for the second data set were mixed on a day of unusually high humidity (for the desert). The

presence of moisture evidently caused the propellant to degas more than usual, and this apparently caused the higher overall burn rates.

TABLE XII

Burn Rate Results for RDX and RDX-d_6 CW5 Propellants at 1000 psi.[a]

Set I		Set II			
RDX-CW5 (r_H)[b]	RDX-d_6-CW5 (r_D)[b]	RDX-CW5 (r_H)[b]		RDX-d_6-CW5 (r_D)[b]	
0.162	0.125	0.241	0.253	0.193	0.179
0.164	0.135	0.229	0.218	0.196	0.188
0.143	0.135	0.252	0.245	0.191	0.188
0.156	0.136	0.227	0.238	0.173	0.184
0.156	0.140	0.257			
$\bar{r}_H = 0.156 \pm 0.010$	$\bar{r}_D = 0.134 \pm 0.005$	$\bar{r}_H = 0.240 \pm 0.010$		$\bar{r}_D = 0.187 \pm 0.006$	
$KDIE = \left(\frac{\bar{r}_H}{\bar{r}_D}\right) = 1.16 \pm 0.05$		$KDIE = \left(\frac{\bar{r}_H}{\bar{r}_D}\right) = 1.29 \pm 0.05$			
Average KDIE[c] = 1.24 ± 0.05					

[a] Reported error is at the 95% confidence level. [b] Values reported in in/s.
[c] Weighted average for data sets I and II.

It is important to note that each data set is self consistent. In each data set both the RDX-CW5 and RDX-d_6-CW5 propellants were prepared under identical conditions using the same ingredients, the cured pellets were burned on the same day under identical conditions, and the data were reduced in the

same manner. Therefore, any differences in burn rates between the RDX-CW5 and RDX-d_6-CW5 propellants are due strictly to the effect of deuterium substitution on the rate limiting process. Consequently, the differences in the KDIE values for the two data sets represent simple statistical variations. Thus, it should be valid to average the two KDIE values.

The data in Tables XI and XII clearly demonstrate an isotope effect for both HMX and RDX CW5 propellant mixtures. The magnitude of the KDIE for HMX-CW5 of 1.29 ± 0.07 is almost identical to that of the pure HMX. The KDIE for RDX-CW5 of 1.24 ± 0.05 is statistically not significantly different at the 95% confidence level from the value for the pure RDX of 1.31 ± 0.03. These data provide evidence that the mechanisms which control the combustion of the pure HMX and RDX continue to control the combustion of the HMX and RDX CW5 propellants. Therefore, a C-H bond rupture during the condensed phase decomposition appears to be the rate controlling process in the combustion of both HMX and RDX CW5 propellant mixtures.

KDIE in PB Propellant Mixtures

The burn rate results for normal and deuterium labeled HMX and RDX PB propellant mixtures are listed in Table XIII. The burn rate of PB propellants containing commercial grade HMX and RDX were measured, giving mean values of 0.155 ± 0.007 in/s and 0.177 ± 0.006 in/s, respectively. The commercial grade results appear to confirm the significantly lower HMX-PB burn rate when compared to the RDX-PB and previous model propellant burn rates.

The KDIE of 1.20 ± 0.04 for the RDX-PB propellant mixture is statistically different at the 95% confidence level from the KDIE value of 1.31 ± 0.03 for the pure RDX. This decrease in isotope effect could be due to a large number of

factors. Unlike the CW5 propellant mixtures, the PB propellants burn in a very heterogeneous manner producing large amounts of carbonaceous residue. This residue tends to remain on the surface of the burning propellant, possibly causing an increase in the burning surface temperature due to increased heat feedback from the flame to the burning surface. This increase in the local temperature of the surface at which the RDX decomposition takes place would be expected to result in a smaller KDIE value.

TABLE XIII

Burn Rate Results for HMX, HMX-d_8, RDX and RDX-d_6 PB Propellants at 1000 psi.[a,b]

HMX-PB (r_H)[c]	HMX-d_8-PB (r_D)[c]	RDX-PB (r_H)[c]	RDX-d_6-PB (r_D)[c]
0.124	0.104	0.193	0.169
0.109	0.114	0.189	0.156
0.112	0.110	0.195	0.160
0.116	0.107		0.157
0.111	0.110		0.162
$\bar{r}_H = 0.114 \pm 0.007$	$\bar{r}_D = 0.109 \pm 0.005$	$\bar{r}_H = 0.192 \pm 0.008$	$\bar{r}_D = 0.161 \pm 0.006$
$KDIE = \left(\frac{\bar{r}_H}{\bar{r}_D}\right) = 1.05 \pm 0.05$		$KDIE = \left(\frac{\bar{r}_H}{\bar{r}_D}\right) = 1.20 \pm 0.04$	

[a] Reported error is at the 95% confidence level. [b] PVC was used as the burning inhibitor for all pellets. [c] Values reported in in/s.

The decrease in the magnitude of the KDIE also could be the result of a change in the RDX decomposition mechanism. This change might be a new rate

limiting step other than a C-H bond rupture (e.g., C-N), or it may be the introduction of a rate limiting process in addition to the C-H bond rupture. Finally, the difference in KDIE values may simply be due to a statistically inaccurate estimate of the RDX-PB propellant isotope effect value caused by a small sample size.

The RDX-PB KDIE of 1.20 falls between the primary and secondary estimates of 1.29 and 1.14, respectively, at 673 K; thus it is difficult to assign this effect to either a C-H or a C-N bond rupture. Because of the fact that all previous RDX decomposition and combustion studies indicate a rate limiting C-H bond rupture and the fact that the KDIE is larger than the estimated secondary effect, I would venture to say that the KDIE for the combustion of RDX-PB propellants is due to a rate limiting C-H bond rupture. However, the assignment is tenuous.

The overall linear burn rates for the HMX-PB propellant as shown in Table XIII are significantly less than for the RDX-PB propellant and all the CW5 propellant mixes. Furthermore, the HMX-PB propellant exhibits a KDIE of only 1.05 ± 0.05, which is much smaller than for all the other propellants in this study. These data indicate a significant change in combustion mechanism between pure HMX and the HMX-PB propellant. Although the isotope effect appears to be real and its value falls well below the estimated secondary effect value, one cannot rule out the possibility that the observed effect is simply a very small primary effect. Thus, from the data available it is impossible to make any kind of assignment of a rate limiting process for HMX-PB propellant combustion.

Interestingly, the "mixed melt" region of HMX decomposition observed by Shackelford et al.[19] exhibited an isotope effect very close to unity. One could speculate that the small KDIE value for the HMX-PB propellant was due to the majority of HMX decomposition occurring in the mixed melt as opposed to either

the solid or liquid phase. This in turn could be the result of the heterogeneous nature of the PB propellant burning.

PROPELLANT BURNING SURFACE AND FLAME CHARACTERISTICS

Kubota,[71] studying the combustion of a nitramine based propellant consisting of 80% HMX or RDX and 20% polyurethane binder (28% by weight oxygen), found that the burning propellant exhibited a two stage flame consisting of a preparation zone (dark zone) directly above the burning surface and below a luminous flame zone. He also found that the thickness of this preparation zone varied with pressure from approximately 0.3 cm at 294 psi (20 atm) to roughly 0.03 cm at 735 psi (50 atm).

In burn rate experiments with our CW5 formulation, which differs from Kubota's propellant in that it contains an energetic plasticizer (TMETN) and a binder with a slightly higher oxygen content (crosslinked R-18 polymer, 37% by weight oxygen), we observed no preparation zone at pressures ranging from 200 to 1500 psi. Figure 17 is indicative of the flame structure observed for all CW5 propellants over the pressure range studied.

A propellant (RRHR-18), identical to Kubota's with the exception that it employed a binder composed of crosslinked R-18 polymer, was prepared and burned at various pressures. There was no significant difference between the burn rates of the RRHR-18 and CW5 propellants. However, at pressures below 750 psi, the RRHR-18 propellants clearly exhibited the two-stage flame observed by Kubota.[71] Furthermore, the preparation zone of the RRHR-18 flame (Fig. 18) decreased with increasing pressure in agreement with the previous study. Additionally, the RRHR-18 flame was more diffuse and significantly lower in intensity than the CW5 flame.

The position of the luminous flame is a dynamic balance between the

rate of production of gaseous reactants at the burning surface and the rate of progression of the flame front.[72,86] When the rate of oxidation reactions in the luminous flame and thus the rate of progression of the flame front exceeds the rate of production of gaseous reactants, the luminous flame moves toward the burning surface until a steady state is achieved. The presence of the energetic plasticizer TMETN in the formulated propellant appears to increase the production of gaseous oxidizing species by the burning surface. This in turn accelerates the rate of the exothermic oxidation reactions in the luminous flame such that, as shown by the CW5 propellants, the flame front moves essentially to the burning surface.

The structure of the CW5 propellant flame suggests that the oxidation reactions in the luminous flame are consuming the gaseous reactants as soon as they are produced by the burning surface, thus implying that the rate of condensed-phase decomposition controls global propellant burn rate.

The extinguished burning surfaces of HMX and RDX CW5 and RRHR-18 propellants are shown in Figures 19–34. The extinguished surfaces for the HMX based propellants (Figs. 19–26) clearly indicate a heterogeneous burning surface. The craters, which cover the extinguished surface, average 30 μm in diameter, and match closely with the weight median diameter of 26 μm for the commercial grade HMX used in these propellants. As has been previously suggested,[67] our data indicate that the burning surface consists of solid particles of HMX resting in a binder melt layer. When this surface was extinguished via rapid depressurization, the melt layer solidified and the HMX particles burned away leaving the observed craters. This observation is in contrast with the extinguished burning surface of pressed pellets of HMX which exhibit a molten layer ranging in thickness from 5 μm at 1000 psi to 20 μm at 250 psi.[87]

Although they exhibit different flame structures there appears to be very little difference between the burning surface of the HMX-CW5 and HMX-RRHR-18 propellants. The only observable difference, albeit small, is a slightly more crystalline solidified binder melt layer in the RRHR-18 propellant (Fig. 26) than in the CW5 propellant (Fig. 22).

The proposed structures of the flame and burning surface for the HMX CW5 and RRHR-18 propellants are shown in Figures 35a and b, respectively. Previous microcinematography investigations[81] of the burning surface of HMX based propellants similar to our CW5 and RRHR-18 formulations have shown the HMX particles to be coated with what appears to be a molten layer. The relatively poor resolution of the high speed video system used in our experiments did not allow us to confirm this observation. The results for the extinguished HMX propellants indicate that the HMX remains essentially intact during the condensed-phase decomposition reactions and only in the gas phase do its decomposition products react with products from the decomposition of the binder. Because of the apparent melt layer on the surface of the HMX particles it is likely that decomposition reactions are occurring both in the solid and liquid phase during propellant combustion.

The quenched burning surfaces of the RDX based propellants (Figs. 27–34) show relatively homogeneous surfaces consisting of a crystalline solid covered by varying amounts of carbonaceous residue. The RDX, which liquefies at 473 K compared to 553 K for HMX, apparently melts along with the binder, giving a uniform liquid layer. This is similar to the melt layer observed on the extinguished surfaces of RDX pressed pellets.[87] When this liquid burning surface is quenched, it produces the observed crystalline surface.

As with the HMX, the RDX CW5 and RRHR-18 extinguished surfaces are essentially the same. The only noticeable difference is the presence of disk

shaped carbon residue on the surface of the RRHR-18 propellant (Fig. 23). The amount and character of the carbonaceous residue, however, were not consistent from sample to sample and apparently it is significantly affected by the quenching process.

The proposed surface and flame structures for the RDX-CW5 and RDX-RRHR-18 propellants are shown in Figures 25c and d, respectively. It is clear from the data presented that the decomposition of RDX occurs in the liquid-phase. Interestingly, even though the molten RDX was in intimate contact with the liquid binder there was no apparent effect on the rate controlling processes as shown by our isotope effect studies.

Extinguished PB propellant samples were studied with an electron microscope. However, because of the extensive amount of residue on the surface of the propellant, it was impossible to distinguish between the burning surface and the carbon residue. Previous studies with an HMX-PB formulation[67] indicate a heterogeneous burning surface composed of HMX particles covered by a molten layer sitting in a binder melt layer. The data given by Beckstead and McCarty[67] and obtained by ourselves unfortunately do not allow us to determine in what phase the HMX decomposition primarily takes place. Unfortunately, there is no information indicating the character of the RDX-PB propellant burning surface as was the case with HMX-PB. However, one can speculate that, considering the similar isotope effects with the CW5 propellant, the surface is likely to be a molten layer of RDX and binder.

The flame of the PB propellants was difficult to observe because of the presence of sheets of binder residue which stacked one on top of the other as shown in Figure 35e. These wafers of residue forced the flame to the sides of the propellant and thus made it impossible to determine the presence or absence of a two stage flame.

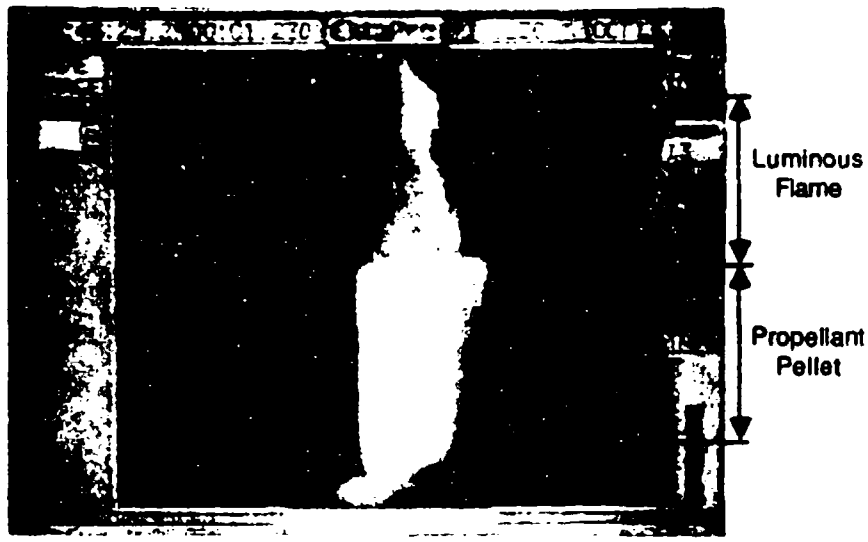

FIGURE 17. Flame structure for HMX and RDX CW5 propellant formulations.

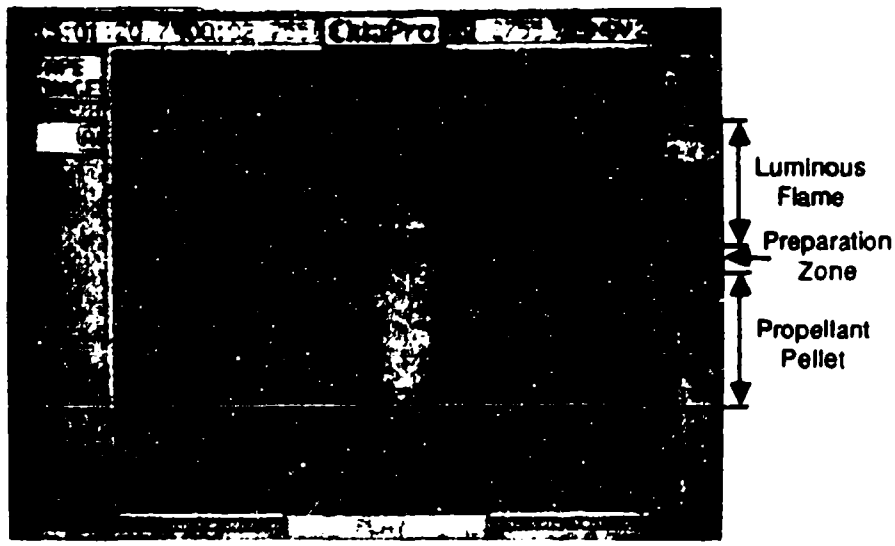

FIGURE 18. Two stage flame structure observed for HMX and RDX RRHR-18 propellants

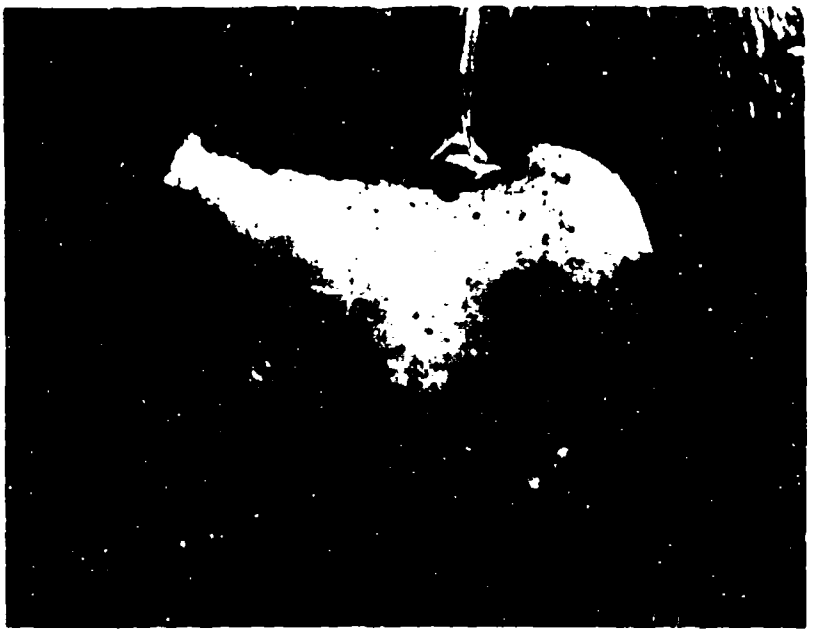

FIGURE 19. Optical Mircograph of an extinguished HMX-CW5 propellant. Magnification is 10 times.

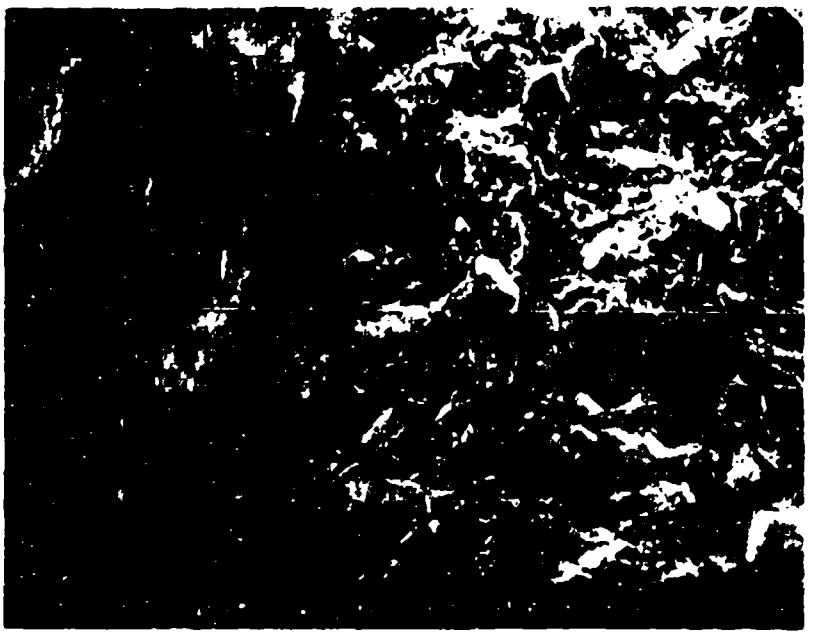

FIGURE 20. An Electron Micrograph of the edge of the extinguished burning surface from a HMX-CW5 propellant. Magnification is 147 times. Burning surface is on the left and unburned propellant is on the right.

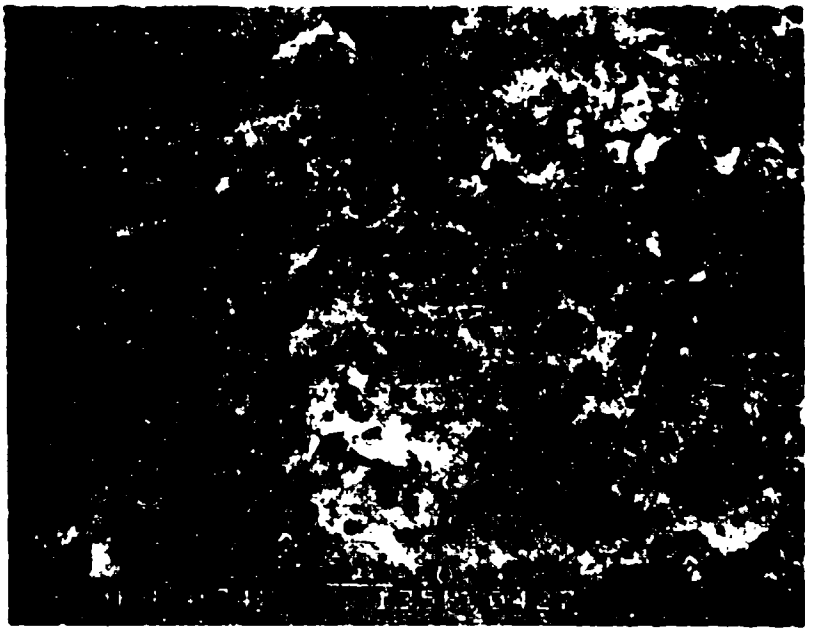

FIGURE 21. An Electron Mircograph of the extinguished burning surface from a HMX-CW5 propellant. Magnification is 74 times

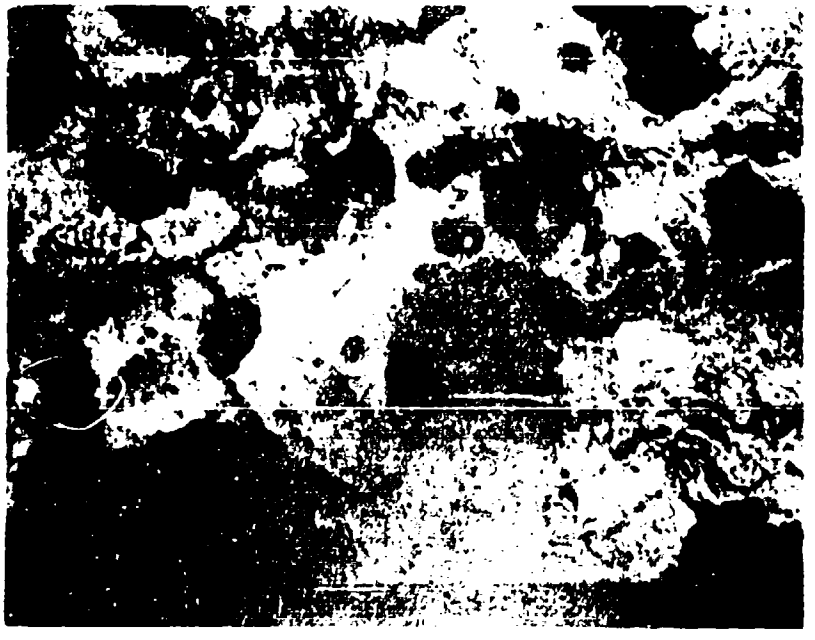

FIGURE 22. An [illegible] of the extinguished [illegible] Figure 11 Magnification is [illegible]

FIGURE 23. Optical Mircograph of an extinguished HMX-RRHR-18 propellant. Magnification is 10 times.

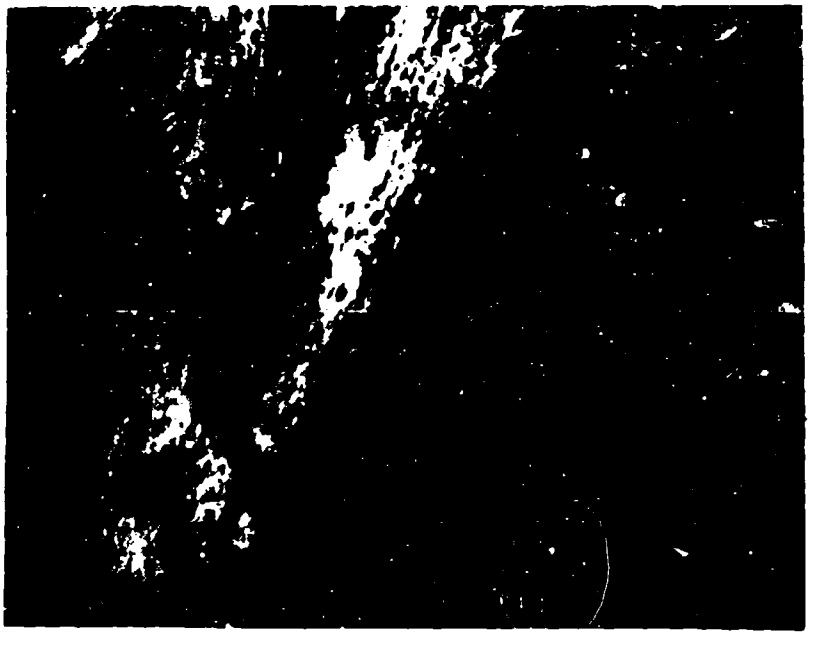

FIGURE 24. An Electron Micrograph of the edge of the extinguished burning surface from a HMX-RRHR-18 propellant. Magnification is 73 times. Burning surface is on the left and unburned propellant is on the right.

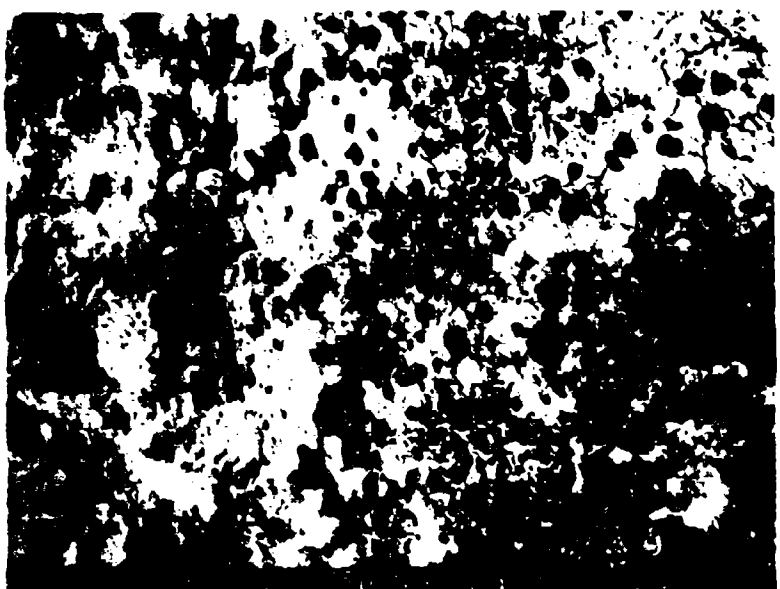

FIGURE 25. An Electron Mircograph of the extinguished burning surface from a HMX-RRHR-18 propellant. Magnification is 124 times.

FIGURE 26. An Electron Mircrograph of the extinguished burning surface from a HMX-RRHR-18 propellant. Magnification is 250 times.

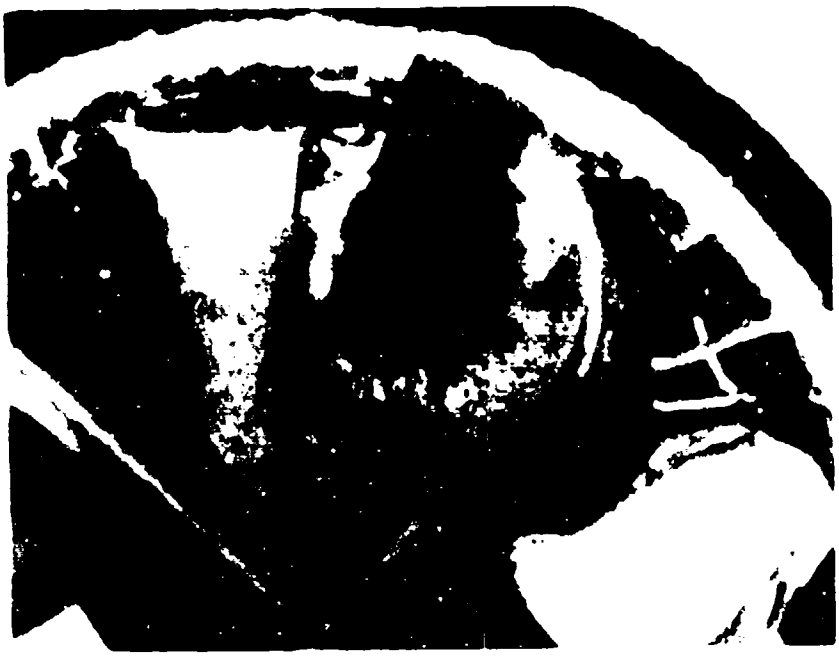

FIGURE 27. Optical Mircograph of an extinguished RDX-CW5 propellant. Magnification is 10 times. Cross section slice shown on the left.

FIGURE 28. An Electron Micrograph of the edge of the extinguished burning surface from a RDX-CW5 propellant. Magnification is 121 times. E rning surface is on the top and unburned propellant is on the bottom.

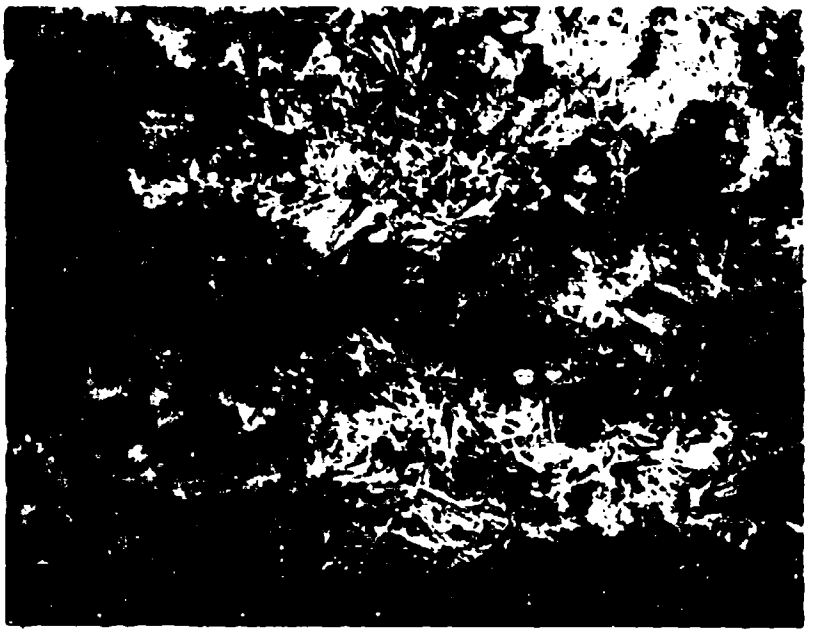

FIGURE 29. An Electron Mircograph of the extinguished burning surface from a RDX-CW5 propellant. Magnification is 127 times.

FIGURE 30. An Electron Mircrograph of the extinguished burning surface from Figure 17. Magnification is 380 times.

FIGURE 31. Optical Mircograph of an extinguished RDX-RRHR-18 propellant. Magnification is 10 times.

FIGURE 32. An Electron Micrograph of the edge of the extinguished burning surface from a RDX-RRHR-18 propellant. Magnification is 122 times. Burning surface is on upper left and unburned propellant is on lower right.

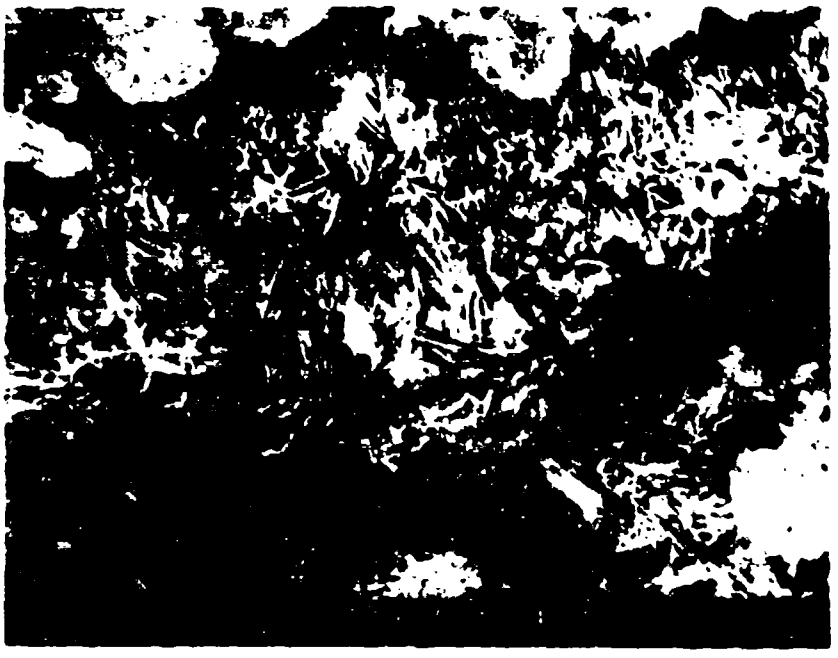

FIGURE 33. An Electron Mircograph of the extinguished burning surface from a RDX-RRHR-18 propellant. Magnification is 136 times.

FIGURE 34. An Electron Mircrograph of the extinguished burning surface from a RDX-RRHR-18 propellant. Magnification is 500 times.

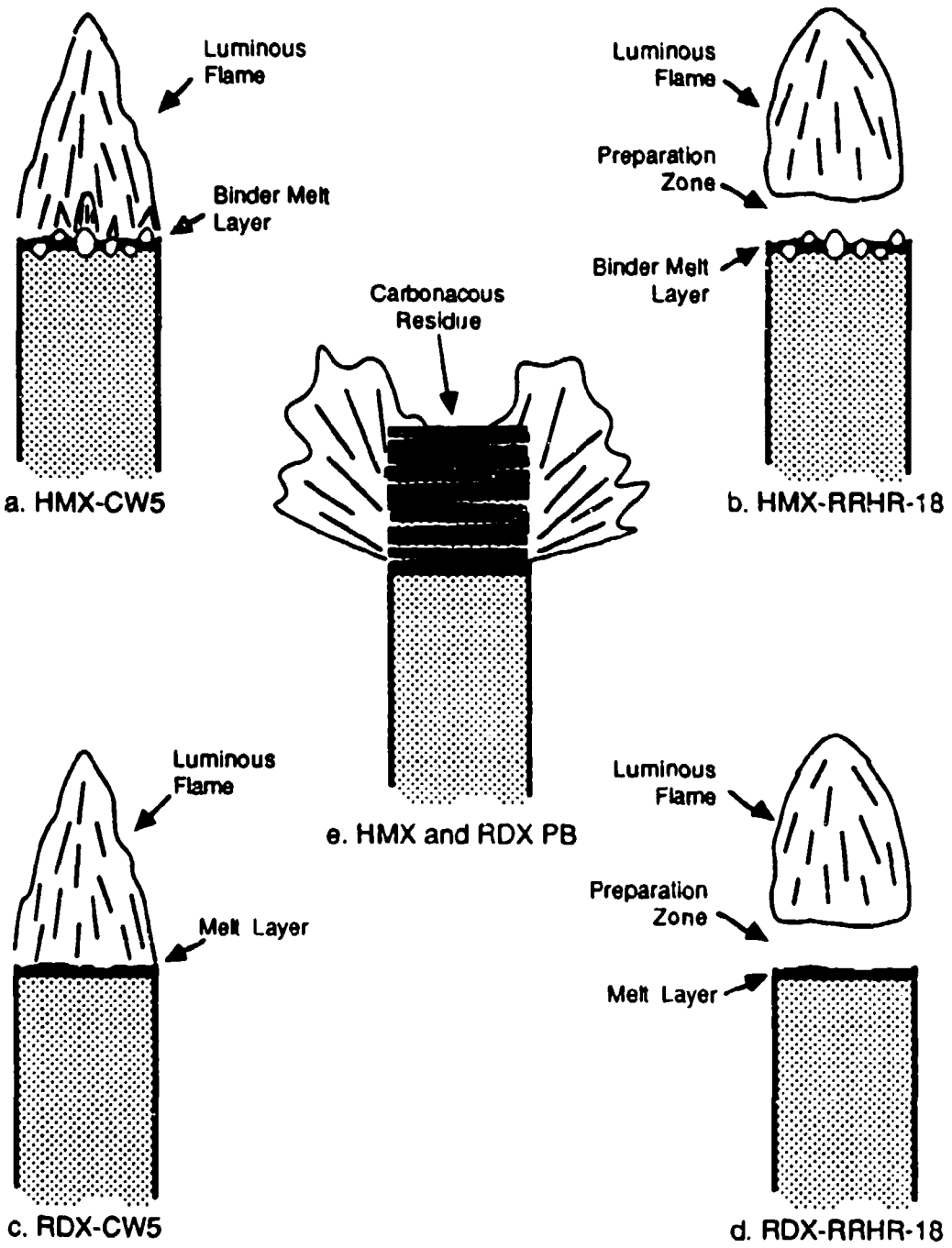

Figure 35. Propellant Flame Structure

β → δ PHASE TRANSITION

HMX in the solid is held together by strong intermolecular coulombic attractions which account for its high density and high melting point.[88] HMX at room temperature is in the β crystalline form which is essentially a chair configuration consisting of the four carbons and two opposite ring nitrogens in a plane with the remaining nitramine units above and below the plane. Above 436 K at atmospheric pressure the β-HMX converts to the high temperature form, δ-HMX.[89] The configuration of δ-HMX is best described as chair–chair. Work by Brill and Karpowicz[90] has shown that the activation energy and Arrhenius preexponential factor for the HMX β → δ phase transition and those for the thermal decomposition of HMX in the condensed phase are essentially the same within experimental error. From their results they concluded that the chemical decomposition of the HMX appears to be controlled by the breakdown of intermolecular forces in the condensed phase.

The results of Brill and Karpowicz[90] imply that the KDIE observed by ourselves and others[16,19,20] are not the consequence of a covalent bond rupture as had originally been concluded. If the breakup of intermolecular forces in the crystal were the cause of the KDIE in HMX then one would expect to observe a significant isotope effect in the HMX β → δ phase transition. However, this appears not to be the case.

The β → δ phase transition for HMX and HMX-d_8 was investigated using differential scanning calorimetry (DSC). The onset of the HMX and HMX-d_8 phase transition endotherm at a scanning rate of 5.00 deg/min occurred at 448.9 ± 1.5 K and 447.0 ± 1.6 K respectively. In addition, the enthalpy of transition for HMX was approximately 7.5 ± 1.2 cal/g and that for HMX-d_8 was approximately 7.0 ± 0.8 cal/g.

The DSC data qualitatively demonstrate the absence of a significant

positive isotope effect in the $\beta \rightarrow \delta$ phase transition. In fact, the data imply that the rate of the HMX-d_8 phase transition may be slightly greater than that of HMX. This observation may provide some explanation for the KDIE very close to unity observed for the decomposition of HMX in the mixed melt.[19] It must be noted that the DSC results represent relatively few measurements and further work is needed to establish the actual effect of deuterium substitution on the $\beta \rightarrow \delta$ phase transition.

Additionally, if the conclusions of Brill and Karpowicz[90] were correct then one would expect significant differences in the intermolecular attractions in HMX versus HMX-d_8. This, in turn, would manifest itself as differences in the crystal structures of HMX and HMX-d_8. Recently a comparison study of the crystal structures of β-HMX and β-HMX-d_8 was conducted.[91] It was found that there were only a few very minor differences in the inter- and intramolecular distances. These differences could account for the small effect of deuterium substitution on the phase transition, but they were not great enough to generate isotope effects on the order of those observed in HMX decomposition and combustion.

From the data presented, it would appear that the breakup of the intermolecular forces in HMX is not the rate controlling process in decomposition and combustion. Furthermore, RDX decomposes primarily in the liquid phase, and consequently the breakup of intermolecular forces cannot be the rate controlling process. Yet RDX exhibits KDIE of similar magnitude to those observed for the decomposition of HMX. Thus, it seems unlikely with compounds as similar as HMX and RDX that the decomposition for one would be controlled by the breakup of intermolecular forces, and the other would be controlled by a covalent bond rupture.

CONCLUSIONS

Our research has confirmed the presence of significant isotope effects in the combustion of HMX and RDX. More importantly, we have demonstrated the existence of significant KDIEs in the combustion of model nitramine propellants. The consistency between the effects of the pure nitramines and those for the HMX and RDX CW5 and RDX-PB propellants indicates similar rate controlling processes. Assuming the rate of condensed-phase decomposition controls the rate of combustion, then the KDIEs observed for the pure nitramines and the above propellants appear to be the result of a rate controlling C-H bond rupture. The combustion of the HMX-PB propellant shows an isotope effect value significantly less than the pure nitramine, indicating a considerable change in the rate controlling process.

This report is particularly significant in extending previous findings from pure oxidizers to propellant systems which are more realistic with respect to additional ingredients which would likely complicate the combustion mechanism. In spite of these ingredients' participation in the global mechanism, evidence has been given that the combustion of the nitramine ingredient in most cases controls the global burn rate of the model propellant.

These results represent the first *in-situ* studies of the rate limiting processes in nitramine propellant combustion. Furthermore, these studies represent some of the first attempts at applying the technique of KDIEs to high temperature combustion. Because of the limited experimental data, the

observed KDIEs can only be evaluated if certain fundamental assumptions are made. Consequently, the assignments of these KDIE must be treated with care until they can be verified by other methods.

REFERENCES AND NOTES

1. Seymor, K. M. *Encyclopedia of Explosives and Related Items*; Picatinny Arsenal: Dover, NJ, 1966; Vol. 3.

2. Seymor, K. M. *Encyclopedia of Explosives and Related Items*; Picatinny Arsenal: Dover, NJ, 1980; Vol. 9

3. Sutton, G. P.; Ross, D. M. *Rocket Propulsion Elements*; John Wiley & Sons: New York, 1976; Chapters 10-12.

4. Reference 3, Chapter 2.

5. Robertson, J. B. *Trans. Faraday Soc.* **1949**, *45*, 85-93.

6. Schroeder, M. A., *CPIA Publication 308*, **1979**, *Vol. II*, 17-34.

7. Schroeder, M. A., *CPIA Publication 329*, **1980**, *Vol. II*, 493-508.

8. Schroeder, M. A., *CPIA Publication 347*, **1981**, *Vol. II*, 395-413.

9. Schroeder, M. A., "Critical Analysis of Nitramine Combustion Data: Some Suggestions for Needed Research Work", ARBRL-MR-3181, AD-A116194, 1982.

10. Schroeder, M. A., "Critical Analysis of Nitramine Decomposition Data: Preliminary Comments on Autoacceleration and Autoinhibition in HMX and RDX Decomposition", ARBRL-MR-03370, 1984; *Chem. Abstr.* **1985**, *102*, 206114.

11. Schroeder, M. A., *CPIA Publication 412*, **1984**, *Vol. II*, 595-614.

12. Schroeder, M. A., "Critical Analysis of Nitramine Decomposition Data: Activation Energies and Frequency Factors for HMX and RDX", BRL-TR-2673, 1985.

13. Schroeder, M. A., "Critical Analysis of Nitramine Decomposition Data: Product Distributions from HMX and RDX Decomposition", BRL-TR-2659, 1985.

14. Boggs, T. L. in *Fundamentals of Solid Propellant Combustion*, Kuo, K. K.; Summerfield, M, Eds.; Progress in Astronautics and Aeronautics Series,

Vol. 90; American Institute of Aeronautics and Astronautics: New York, 1984; Chapter 3.

15. Fifer, R. A. In *Fundamentals of Solid Propellant Combustion*, Kuo, K. K.; Summerfield, M, Eds.; Progress in Astronautics and Aeronautics Series, Vol. 90; American Institute of Aeronautics and Astronautics: New York, 1984; Chapter 4.

16. (a) Shackelford, S. A. ; Coolidge, M. B.; Goshgarian, B. B.; Rogers, R. N.; Janney, J. L.; Ebinger, M. H.; Flanigan, D. A.; Askins, R. E., *CPIA Publication 383, 1983, Vol. I*, 571-580; (b) Shackelford, S. A. *Int.-Jahrestag.-Fraunhofer-Inst. Treib-Explosivst. 17th (Anal. Propellants Explos.: Chem. Phys Methods)* **1986**, 23/1-23/10. (c) Shackelford, S. A.; Goshgarian, B. B.; Chapman, R. D.; Askins, R. E.; Flanigan, D. A.; Rogers, R. N., *Propellants Explos. Pyrotech.*, in press.

17. Shackelford, S. A.; Rodgers, S. L.; Coolidge, M. B.; Askins, R. E., *CPIA Publication 412*, **1984**, *Vol. I*, 615-621.

18. (a)Bulusu, S.; Autera, J. R.; Anderson, D. A.; Velicky, R. W. *Deuterium Kinetic Isotope Effect: An Experimental Probe for the Molecular Process Governing the Initiation of TNT and RDX*; Proc. 1984 Army Science Conference (June 1984), Vol. I, 93-106. (b) Bulusu, S; Autera, J. R. *J. Energ. Mater.* **1983**, *1*, 133-140.

19. Shackelford, S. A.; Coolidge, M. B.; Goshgarian, B.B.; Loving, B. A. ; Rogers, R. N.; Janney, J. L.; Ebinger, M. H. *J. Phys. Chem.* **1985**, *89*, 3118-3126.

20. Bulusu, S.; Weinstein, D. I.; Autera, J. R.; Velicky, R. W. *J. Phys. Chem.* **1986**, *90*, 4121-4126.

21. Klumpp, G. W. *Reactivity in Organic Chemistry* ; John Wiley & Sons: New York, 1982; pp 256-265.

22. Lowry, T. H.; Richardson, K. S. *Mechanism and Theory in Organic Chemistry* ; Harper & Row: New York, 1976; pp 105-111, 120-123.

23. Thornton, E. K.; Thornton, R. T. In *Isotope Effects in Chemical Reactions* ; Collins, C. J. ; Bowman, N. S., Eds.; Van Nostrand Reinhold: New York, 1970; Chapter .

24. Bigeleisen, J.; Mayer, M. G. *J. Chem. Phys.* **1947**, *15*, 261-267.

25. Glasstone, S.; Laidler, K.; Eyring, H. *The Theory of Rate Processes;* McGraw-Hill: New York, 1941.

26. Westheimer, F. H. *Chem. Rev.* **1961**, *61*, 265-273.

27. Bigeleisen, J.; Wolfsberg, M. *Adv. Chem. Phys.* **1958**, *1*, 15-76.

28. Bigeleisen, J. *Science* **1965**, 147, 463-471.

29. Saunders, W. H. *Surv. Prog. Chem.* **1966**, *3*, 109-146.

30. Goldstein, M. J. *Science* **1966**, *154*, 1616-1621.

31. Weston, R. E. *Science* **1967**, *158*, 332-342.

32. Van Hook, W. A. In *Isotope Effects in Chemical Reactions* ; Collins, C. J. ; Bowman, N. S., Eds.; Van Nostrand Reinhold: New York, 1970; Chapter 1.

33. Saunders, W. H. In *Investigations of Rates and Mechanisms of Reactions* ; Lewis, E. S., Ed.; John Wiley & Sons: New York, 1968; Chapter 5.

34. This name arises from the fact that the molecule will still possess this amount of energy at absolute zero.

35. Moore, W. J. *Physical Chemistry* ; 4th ed.;Prentice-Hall: Englewood Cliffs, New Jersey, 1972; Chapter 5. For the experiments discussed in this thesis, the reaction temperatures ranged up to approximately 673 K. When looking at the Boltzmann distribution at 673 K for the most common vibrational frequencies of hydrogen and deuterium , it appears that in most cases well over 90% of the molecules occupy the n = 0 ground state vibrational level. Thus, it should be a reasonable approximation to treat reactions at temperatures up to 673 K as if all molecules were in the n = 0 state.

36. Kwart, H. *Acc. Chem. Res.* **1982**, *15*, 401-408.

37. Benson, S. W. *The Foundations of Chemical Kinetics* ; McGraw-Hill: New York, 1960; Chapter 4.

38. Schneider, M. E.; Stern, M. J. *J. Am. Chem. Soc.* **1972**, *94*, 1517-1522.

39. The deBroglie wavelength (λ) of a particle is given by

$$\lambda = \frac{h}{mv}$$

where h is Plank's constant, m is the mass of the particle, and v is the particles velocity. Because the deBroglie wavelength is inversely proportional to mass, the wavelength of protium is twice that of deuterium for the same value of v.

40. Sunko, D. E.; Borcic, S. In *Isotope Effects in Chemical Reactions* ; Collins, C. J. ; Bowman, N. S., Eds.; Van Nostrand Reinhold: New York, 1970; Chapter 3.

41. Wolfsberg, M.; Stern, M. J. *Pure Appl. Chem.* **1964**, *8*, 225-242.

42. Stern, M. J.; Wolfsberg, M. *J. Chem. Phys.* **1966**, *45*, 2618-2629. If there is no change in the force constants when going from reactants to activated complex, only small secondary KDIE, arising from non zero point energy contributions, will be observed. In general, the upper limits for secondary KDIE of this type are 1.015 and 1.002 per deuterium atom for α and β deuteriums respectively.

43. Halevi, E. A. *Prog. Phys. Org. Chem.* **1963**, *1*, 109-221.

44. Streitwieser, A.; Jagow, R. H.; Fahey, R. C.; Suzuki, S. *J. Am. Chem. Soc.* **1958**, *80*, 2326-2332.

45. Shackelford, S. A.; Beckmann, J. W.; Wilkes, J. S. *J. Org. Chem.* **1977**, *42*, 4201-4206.

46. Bawn, C. E. H. In *Chemistry of the Solid State*; Garner, W. E., Ed.; Butterworths Scientific Publications: London, 1955; Chapter 10.

47. Beckmann, J. W.; Wilkes, J. S.; McGuire, R. R. *Thermochim. Acta* **1977**, *19*, 111-118.

48. Dacons, J. C.; Adolph, H. G.; Kamlet, M. J. *J. Phys. Chem.* **1970**, *74*, 3035-3040.

49. Rogers, R. N. *Anal. Chem.* **1967**, *39*, 730-733.

50. Bulusu, S.; Autera, J. R. *J. Energetic Mater.* **1983**, *1*, 177-205.

51. Swanson, J. T. (F. J. Seiler Research Laboratory, U. S. Air Force Academy, CO) personal communication.

52. Chang, M. H.; Crawford, R. J. *Can. J. Chem.* **1981**, *59*, 2556-2567.

53. Rogers, R. N.; Janney, J. L.; Ebinger, M. H. *Thermochim. Acta* **1982**, *59*, 287-298.

54. Silverstein, R. M.; Bassler, G. C. *Spectrometric Identification of Organic Compounds*, 2nd ed.; John Wiley & Sons: New York, 1967; Chapter 3.

55. Trulove, P. C.; Chapman, R. D.; Shackelford, S. A., *CPIA Publication 476*, **1987**, *Vol. I*, 303-308.

56. Bulusu, S.; Graybush, R. J.; Autera, J. R. *Chem. Ind (London)* **1967**, 2177-2178. Interestingly, mass spectral studies of ^{15}N labelled HMX indicate that three fourths of the N-N bonds remain intact during decomposition. However, these results merely indicate that after the first NO_2 group is lost the remainder of the bond breaking occurs in the ring.

57. Weston, R. E. *J. Chem. Phys.* **1957**, *26*, 975-983. The dependence of the magnitudes of isotope effects on pressure is relatively slight at high pressures (> 1 atm) even for gas-phase reactions. The dependence for condensed-phase reactions should be even less.

58. Siele, V. I.; Warman, M.; Gilbert, E. E. *J. Heterocycl. Chem.* **1974**, *11*, 237-239.

59. Gilbert, E. E.; Leccacorvi, J. R.; Warman, M. *ACS Symp. Ser.* **1976**, *22* (Ind. Lab. Nitrations, Symp., 1975), 327-340.

60. Coburn, M. D.; Ott, D. G. *J. Labelled Compd. and Radiopharm.* **1980**, *18*, 1423-1427.

61. Siele, V. I.; Warman, M.; Leccacorvi, J.; Hutchinson, R. W.; Motto, R.; Gilbert, E. E.; Benzinger, T. M.; Coburn, M. D.; Rohwer, R. K.; Davey, R. K. *Propellants Explos. Pyrotech.* **1981**, *6*, 67-73.

62. Bedford, C. D.; Deas, B. D.; Broussard, M. M.; Geigel, M. A. "Preparation Purification of Multigram Quantities of TAX and SEX", 1982, AD-A122816; *Chem. Abstr.* **1983**, *99*, 73150.

63. Chapman, R. D., (Air Force Astronautics Laboratory, Edwards AFB, CA) personal communication, 1985.

64. Rodgers, S. L., (Air Force Astronautics Laboratory, Edwards AFB, CA) personal communication, 1986.

65. Chandler, K. G., (Air Force Astronautics Laboratory, Edwards AFB, CA) personal communication, 1987. The effect of particle size on the burn rate of HMX-CW5 propellant was recently studied. It was shown that a change in HMX particle size from 20 to 100 μ increases the propellant burn rate by only 5%.

66. Edwards, J. T. (Air Force Astronautics Laboratory, Edwards AFB, CA) personal communication, 1987.

67. Beckstead, M. W.; McCarty, K. P. *AIAA J.* **1982**, *20*, 106-115.

68. Kubota, N. *Symp. (Int.) Combust., [Proc.]* **1982**, *19th*, 777-785; *Chem. Abstr.* **1983**, *98*, 218168.

69. Seymour, R. B.; Carraher, C. E. *Polymer Chemistry*; Marcell Dekker, Inc.: New York, 1981; Chapter 7.

70. Huynh-Ba, G.; Jerome, R. *ACS Symp. Ser.* **1981**, *172* (Urethane Chemistry and Applications), 205-217.

71. Kubota, N. *Symp. (Int.) Combust., [Proc.]* **1981**, *18th*, 187-194; *Chem. Abstr.* **1981**, *95*, 172009.

72. Kubota, N. in *Fundamentals of Solid Propellant Combustion*, Kuo, K. K.; Summerfield, M, Eds.; Progress in Astronautics and Aeronautics Series, Vol. 90; American Institute of Aeronautics and Astronautics: New York, 1984; Chapter 1.

73. Reference 37, Chapter 3.

74. Wayne, R. P. in *Comprehensive Chemical Kinetics; Bradford*;C. H.; Tipper, C. F. H., Eds.; Elservier Publishing Company: New York, 1969: Chapter 3.

75. Zhao, X.; Hintsa, E. J.; Lee, Y. T. *J. Chem. Phys.* **1988**, *88*, 801-810.

76. Melius, C. F.; Binkley, J. S. in "Combustion Probes for Solid Nitramines: Workshop Report",Shaw, R. W.; Johnson, S. C.; Adams, G. F., Eds.; June 9-11, 1986, Livermore California, pp. 224-241.

77. Rogers, R. N. *Anal. Chem.* **1972**, *44*, 1336-1337.

78. Rogers, R. N. *Thermochim. Acta* **1974**, *9*, 855-855.

79. Reference 74, Chapter 5.

80. Cohen, N. S.; Price, C. F. *J. Spacecr. Rockets* **1975**, *12*, 608-612.

81. Cohen, N. S.; "Nitramine Propellant Research", Jet Propul. Lab., Pasadena CA, AFOSR-TR-76-1163, (AD-A033034) 1976; *Chem. Abstr.* **1977**, *86*, 192059.

82. Cohen, N. S.; "Nitramine Smokless Propellant Research", NASA-CR-157150, 1977; *Chem. Abstr.* **1978**, *89*, 181931.

83. Kumar, R. N.; Strand, L. D. *J. Spacecr. Rockets* **1977**, *14*, 427-433.

84. Cohen, N. S.; Strand, L. D. *AIAA J.* **1980**, *18*, 968-972.

85. Cohen, N. S.; Lo, G. A.; Crowley. J. C. *AIAA J.* **1985**, *23*, 276-282.

86. Strehlow, R. A. *Combustion Fundamentals*; McGraw-Hill: New York, 1984; Chapter 8.

87. Scwarz, W. W.; Askins, R. E.; Flanigan, D. A. "Nitramine Combustion Final Report", AFRPL-TR-84-012, 1984.

88. Brill, T. B.; Reese, C. O. *J. Phys. Chem.* **1980**, *84*, 1376-1380.

89. Karpowicz, R. J.; Brill, T. B. *AIAA J.* **1982**, *20*, 1586-1591.

90. Brill, T. B. *J. Phys. Chem.* **1982**, *86*, 4260-4265.

91. Trulove, P. C.; Lauderdale, W. J.; Hardcastle, K. I. (California State University, Northridge), unpublished results.